Molecular Cell

Article

Dual Role of Ribosome-Binding Domain of NAC as a Potent Suppressor of Protein Aggregation and Aging-Related Proteinopathies

Graphical Abstract

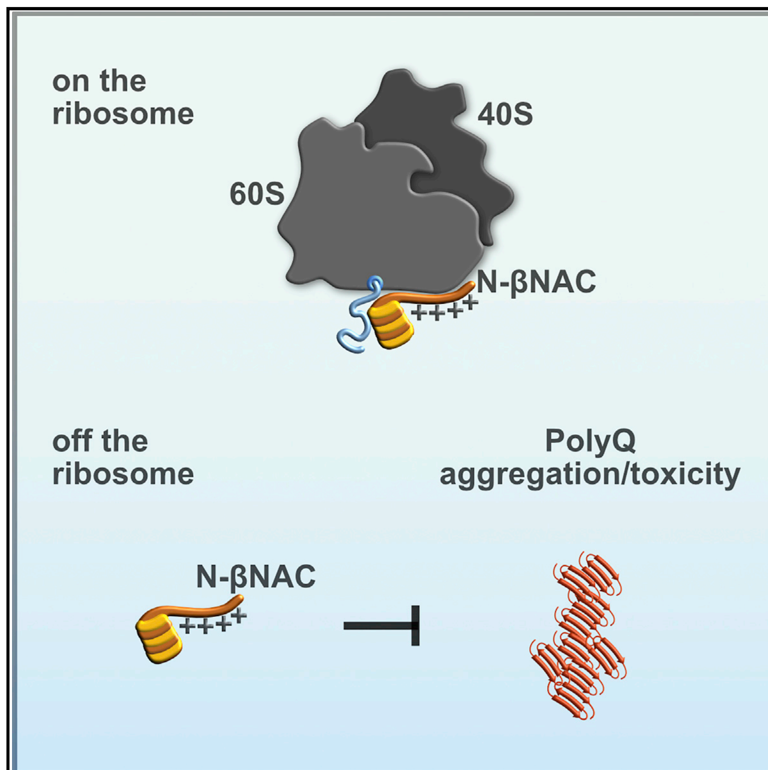

Highlights

- The protein biogenesis factor NAC exhibits broad-spectrum chaperone activity
- NAC exerts a ribosome-independent chaperone function
- The positively charged N terminus of βNAC is a central chaperone entity of NAC
- NAC suppresses aggregation and toxicity of disease-related polyglutamine proteins

Authors

Koning Shen, Martin Gamerdinger, Rebecca Chan, ..., Sheena E. Radford, Judith Frydman, Elke Deuerling

Correspondence

s.e.radford@leeds.ac.uk (S.E.R.),
jfrydman@stanford.edu (J.F.),
elke.deuerling@uni-konstanz.de (E.D.)

In Brief

NAC is a conserved protein biogenesis factor. Shen et al. demonstrate that NAC acts as a chaperone suppressing aggregation and toxicity of human disease-related polyglutamine-expanded proteins. They identify the positively charged domain of βNAC as the critical chaperone domain and show that NAC also acts independent of its ribosome association.

Shen et al., 2019, Molecular Cell *74*, 729–741
May 16, 2019 © 2019 The Authors. Published by Elsevier Inc.
https://doi.org/10.1016/j.molcel.2019.03.012

CellPress

Molecular Cell
Article

Cell Press

Dual Role of Ribosome-Binding Domain of NAC as a Potent Suppressor of Protein Aggregation and Aging-Related Proteinopathies

Koning Shen,[1,4,5] Martin Gamerdinger,[2,4] Rebecca Chan,[1] Karina Gense,[2] Esther M. Martin,[3] Nadine Sachs,[2] Patrick D. Knight,[3] Renate Schlömer,[2] Antonio N. Calabrese,[3] Katie L. Stewart,[3] Lukas Leiendecker,[2] Ankit Baghel,[1] Sheena E. Radford,[3,*] Judith Frydman,[1,*] and Elke Deuerling[2,6,*]

[1]Department of Biology, Stanford University, Stanford, CA 94305-5430, USA
[2]Department of Biology, University of Konstanz, 78457 Konstanz, Germany
[3]Astbury Centre for Structural Molecular Biology, School of Molecular and Cellular Biology, Faculty of Biological Sciences, University of Leeds, Leeds LS2 9JT, UK
[4]These authors contributed equally
[5]Present address: Department of Molecular and Cell Biology, UC Berkeley, Berkeley, CA 94704, USA
[6]Lead Contact
*Correspondence: s.e.radford@leeds.ac.uk (S.E.R.), jfrydman@stanford.edu (J.F.), elke.deuerling@uni-konstanz.de (E.D.)
https://doi.org/10.1016/j.molcel.2019.03.012

SUMMARY

The nascent polypeptide-associated complex (NAC) is a conserved ribosome-associated protein biogenesis factor. Whether NAC exerts chaperone activity and whether this function is restricted to *de novo* protein synthesis is unknown. Here, we demonstrate that NAC directly exerts chaperone activity toward structurally diverse model substrates including polyglutamine (PolyQ) proteins, firefly luciferase, and Aβ40. Strikingly, we identified the positively charged ribosome-binding domain in the N terminus of the βNAC subunit (N-βNAC) as a major chaperone entity of NAC. N-βNAC by itself suppressed aggregation of PolyQ-expanded proteins *in vitro*, and the positive charge of this domain was critical for this activity. Moreover, we found that NAC also exerts a ribosome-independent chaperone function *in vivo*. Consistently, we found that a substantial fraction of NAC is non-ribosomal bound in higher eukaryotes. In sum, NAC is a potent suppressor of aggregation and proteotoxicity of mutant PolyQ-expanded proteins associated with human diseases like Huntington's disease and spinocerebellar ataxias.

INTRODUCTION

A multifaceted chaperone network guards the integrity of the cellular proteome. This network comprises various conserved families of molecular chaperones operating in all cellular subcompartments to promote the folding and function of their protein substrates and counteract proteotoxicity provoked by protein misfolding and aggregation (Kim et al., 2013). A subset of molecular chaperones is specialized for *de novo* protein folding, including the ribosome-associated complex (RAC) in eukaryotes or trigger factor in bacteria. These systems directly bind to translating ribosomes near the peptide exit tunnel to engage their substrates in a co-translational manner. Installed at the ribosome, they are enabled to assist protein folding at the earliest possible time when nascent chains are just reaching the cytoplasm. These chaperones thus lay the groundwork for the maintenance of protein homeostasis in the cell (Pechmann et al., 2013; Preissler and Deuerling, 2012).

A major factor in eukaryotes that quantitatively associates with translating ribosomes near the peptide exit site is the ubiquitous nascent polypeptide-associated complex (NAC) (Wiedmann et al., 1994). It consists of two different subunits, αNAC and βNAC, that dimerize when their homologous NAC domains form a semi-β-barrel core (Liu et al., 2010; Wang et al., 2010). NAC is an abundant complex expressed at least equimolar relative to ribosomes; thus, most translating ribosomes likely associate with NAC (del Alamo et al., 2011; Raue et al., 2007). Essential for ribosome binding is an ~40 aa domain found specifically in the N terminus of the βNAC subunit (herein N-βNAC). N-βNAC is highly conserved and exhibits a characteristic positive net charge. Deletion of either the first N-terminal 11 amino acids or mutation of a conserved positively charged central motif (RRKxxKK) abolishes ribosome binding in yeast, suggesting that this domain mediates the main ribosomal contact of NAC (Pech et al., 2010; Wegrzyn et al., 2006).

Because of its localization at the ribosomal tunnel exit, a proposed function of NAC is to act as a co-translational molecular chaperone similar to the ATP-independent trigger factor in bacteria. However, only indirect evidence supports this assumption, and mechanistic details of the proposed chaperone activity are entirely unknown (Duttler et al., 2013; Kirstein-Miles et al., 2013; Ott et al., 2015; Wang et al., 2013). Crosslinking data suggest that both NAC subunits can interact with protein clients, but the particular substrate binding site(s) of α- and βNAC and the substrate binding specificity are unknown (Martin et al., 2018; Wang et al., 1995). Further, whether

This is an open access article under the CC BY-NC-ND license (http://creativecommons.org/licenses/by-nc-nd/4.0/).

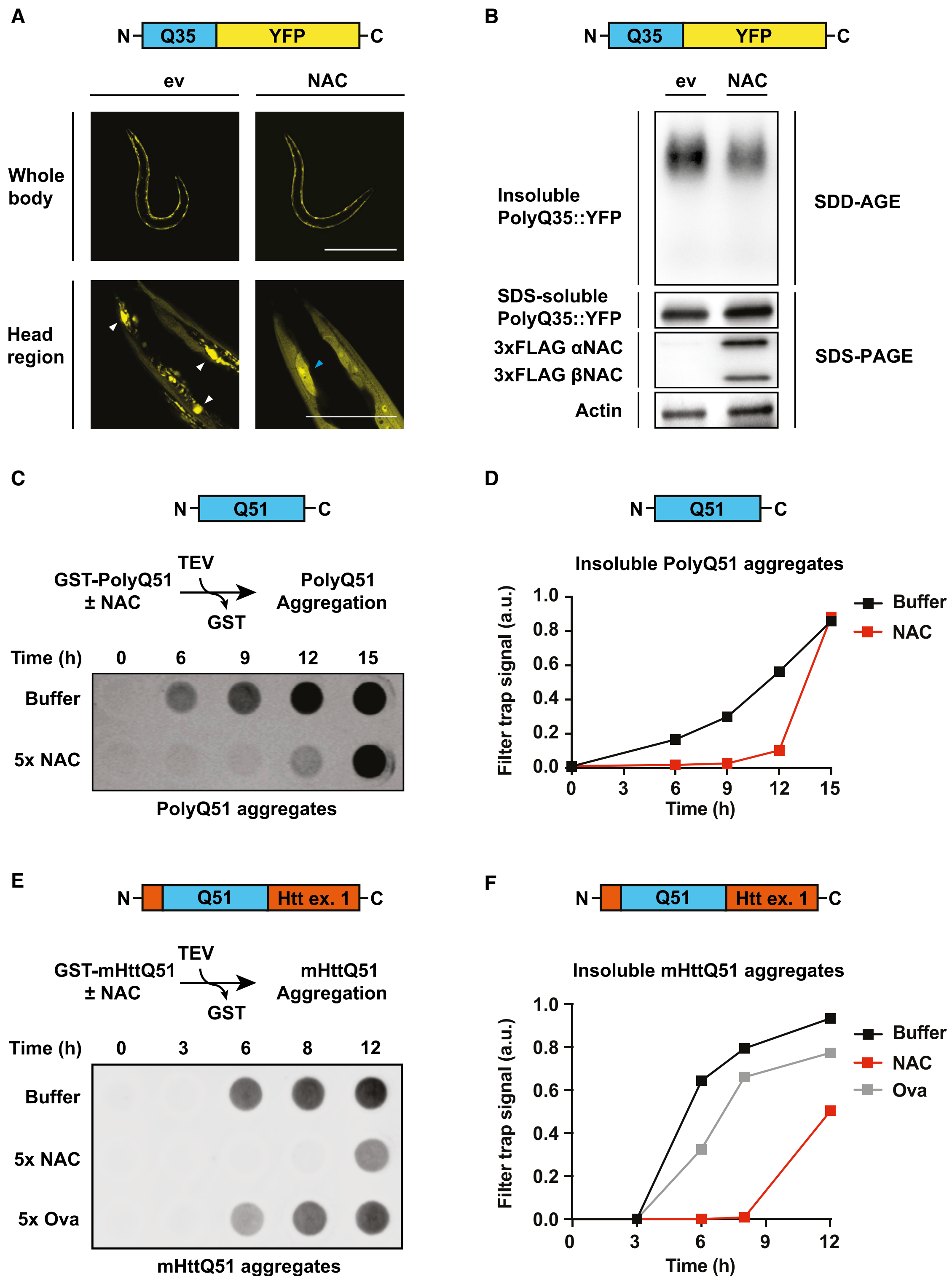

Figure 1. NAC Suppresses Aggregation of Diverse PolyQ Proteins

(A) Fluorescence microscope images of PolyQ35::YFP *C. elegans* worms overexpressing NAC (FLAG-tagged α- and βNAC) in muscle cells. Images were taken at day 3 of adulthood. Scalebar, 500 μm in whole body images and 50 μm in images showing the head region. PolyQ35::YFP aggregates and cell nuclei are indicated by white and blue arrowheads, respectively. ev, empty vector.

(legend continued on next page)

NAC has a function aside from its co-translational ribosomal role is unknown.

Here, we conducted a series of *in vitro* and *in vivo* experiments to explore the potential chaperone function of NAC in greater detail. We found that NAC directly exerts chaperone activity as a holdase toward a set of structurally and physicochemically diverse model substrates. NAC effectively suppresses aggregation of disease-related polyglutamine-expanded (polyQ) proteins and amyloid-β 40 (Aβ40) peptides, as well as denatured firefly luciferase, independent from its ribosome association. Specifically, our data reveal that the ribosome-binding domain N-βNAC represents a central chaperone domain of NAC. Moreover, we found that NAC enhances organismal fitness of PolyQ-expressing *C. elegans* animals and prevents proteostasis collapse in neurons expressing PolyQ-expanded Huntingtin. These data suggest that NAC is a chaperone that acts as a potent modifier of age-related proteinopathies.

RESULTS

NAC Suppresses Aggregation of Diverse PolyQ Proteins

NAC is a major ribosome-binding factor interacting broadly with nascent chains (del Alamo et al., 2011). However, its assumed chaperone function is poorly investigated. A previous study in *C. elegans* showed that depletion of NAC leads to increased aggregation of a model PolyQ protein (Kirstein-Miles et al., 2013). Although loss of NAC causes pleiotropic defects in *C. elegans* (Gamerdinger et al., 2015), this finding raises the possibility that NAC directly exerts a chaperone function on aggregation-prone proteins. In this case, overexpression of NAC should prevent aggregation of PolyQ proteins *in vivo*. Therefore, we used a *C. elegans* strain expressing 35 consecutive glutamine residues fused to YFP (PolyQ35::YFP) in body-wall muscle cells. This PolyQ length is close to the aggregation threshold in *C. elegans* muscle cells, leading to progressive, age-dependent aggregation starting at day 2 of adulthood (Morley et al., 2002). We generated transgenic animals that overexpress FLAG-tagged α- and βNAC under the control of the muscle-specific *myo-3* promoter. PolyQ aggregation was assessed at day 3 of adulthood by fluorescence microscopy as well as semi-denaturing detergent agarose gel electrophoresis (SDD-AGE), which detects high-molecular weight oligomeric PolyQ species (Halfmann and Lindquist, 2008). The overexpression of NAC did not alter the overall morphology of *C. elegans* and expression levels of PolyQ35::YFP (Figure 1A, whole body images). However, we found that overexpression of NAC effectively suppressed PolyQ35::YFP aggregation in worms. This is evident by magnification of the head regions showing diffuse PolyQ35::YFP and less punctate PolyQ35::YFP structures when NAC was overexpressed (Figure 1A, head region images). Consistent with the fluorescence microscopy analysis, we found less insoluble high molecular weight aggregate species in NAC-overexpressing worms by SDD-AGE analysis (Figures 1B and S1A). These data indicate that NAC is a modifier of PolyQ aggregation. To directly test the potential chaperone function of NAC, we employed a peptide composed of 51 consecutive glutamines (PolyQ51) as a model substrate in a well-established *in vitro* aggregation assay. We initiated aggregation of PolyQ51 by cleaving a solubilizing GST tag with TEV protease and detected aggregates over time using a filter trap assay. Addition of purified human NAC strongly delayed the accumulation of PolyQ51 aggregates (Figures 1C and 1D), suggesting that NAC directly acts on the polyglutamine stretch and slows the rate of aggregation.

The aggregation suppression effect of NAC on the pure PolyQ substrate predicts that NAC may also inhibit aggregation of pathogenic proteins harboring an extended PolyQ tract. Thus, we investigated whether NAC prevents aggregation of mutant Huntingtin exon 1, the causative agent in the human neurodegenerative disorder Huntington's disease (Labbadia and Morimoto, 2013). Using the same *in vitro* filter trap aggregation assay, we found that human NAC effectively suppressed aggregation of mutant Huntingtin exon 1 containing a pathogenic stretch of 51 glutamines (mHttQ51), whereas a molar equivalent ovalbumin control showed little effect (Figures 1E and 1F). Aggregation suppression of mHttQ51 by NAC was concentration dependent (Figure S1B) and was also observed, albeit to a lesser extent, with the *C. elegans* form of NAC (Figure S1C). Moreover, we found that NAC did not disaggregate preformed mHttQ51 aggregates *in vitro* (Figure S1D), suggesting that NAC exhibits a holdase function on early aggregation species to prevent further oligomerization, similar to the apical domain of the chaperonin TRiC (Tam et al., 2006).

A second pathogenic PolyQ substrate tested was full-length ataxin-3 harboring a stretch of 78 glutamines (AtxQ78), which causes spinocerebellar ataxia-3 in humans (Matos et al., 2011). Importantly, this protein shares no homology with Huntingtin exon 1 aside from the mutant expansion of a PolyQ repeat and aggregates via a separate kinetic mechanism (Saunders and Bottomley, 2009; Scarff et al., 2015). AtxQ78 exhibits lower aggregation propensity compared to PolyQ51 and mHttQ51, circumventing the requirement of a solubilizing tag. To assess whether NAC also affects AtxQ78 aggregation, we incubated the AtxQ78 substrate in the presence or absence of purified human NAC at 37°C and assessed aggregation by a filter trap

(B) PolyQ35::YFP aggregation in animals as in (A) was further assessed by semi-denaturing agarose gel electrophoresis (SDD-AGE) immunoblot analysis. Total levels of SDS-soluble PolyQ35::YFP and FLAG-tagged NAC subunits were assessed by denaturing SDS-PAGE immunoblot analysis. Actin served as loading control.

(C) Filter trap aggregation assay of PolyQ51 peptide incubated with 5× molar excess of human NAC *in vitro*. Aggregation of GST-PolyQ51 was initiated by cleavage of the GST tag using the TEV protease. SDS-insoluble aggregates were detected with an S-tag antibody.

(D) Quantification of SDS-insoluble PolyQ51 aggregates obtained in filter trap from (C). Data are representative of at least 3 independent biological replicates.

(E) Filter trap aggregation assay of mutant Huntingtin (mHttQ51) incubated with 5× molar excess of human NAC or ovalbumin control (Ova) *in vitro*. Aggregation of GST-mHttQ51 was initiated by cleavage of the GST tag using the TEV protease. SDS-insoluble aggregates were detected with an S-tag antibody.

(F) Quantification of SDS-insoluble mHttQ51 aggregates obtained in filter trap from (E). Data are representative of at least 3 independent biological replicates. See also Figure S1.

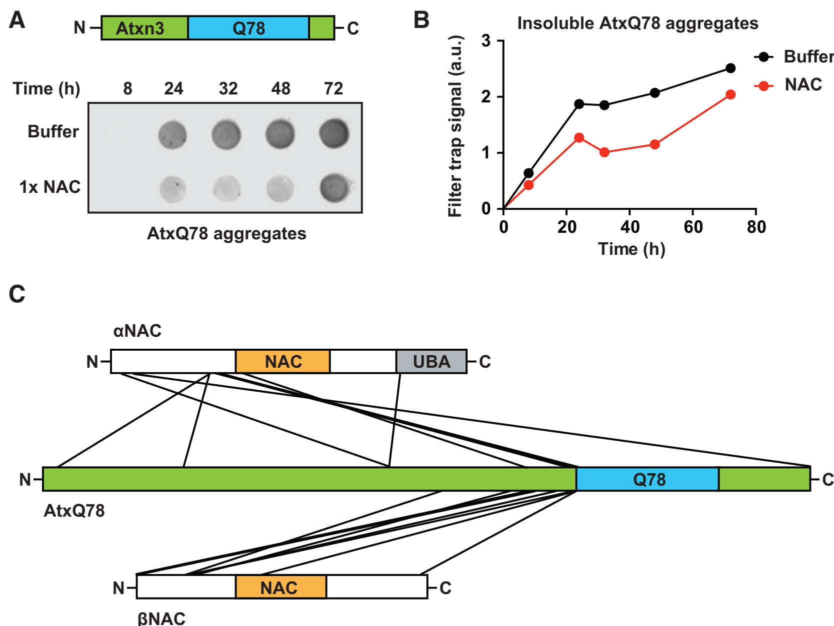

Figure 2. NAC Suppresses Aggregation of Mutant Ataxin-3

(A) Filter trap aggregation assay of full-length Ataxin-3 containing a stretch of 78 glutamines (AtxQ78) incubated with 1× molar excess of NAC at 37°C for the indicated time. SDS-insoluble aggregates were detected with an anti-His antibody.

(B) Quantification of SDS-insoluble AtxQ78 aggregates obtained in filter trap from (A). Data are representative of at least 3 independent biological replicates.

(C) NAC and AtxQ78 were incubated in a 1:1 molar ratio and crosslinked using the homobifunctional crosslinker BS^3. The schematic shows all intermolecular BS^3 crosslinks identified by MS analysis of NAC-AtxQ78 complexes excised from the gel shown in Figure S2C.

See also FigureS2 and Table S1.

assay. Similar to the effect on PolyQ51 and mHttQ51, addition of human NAC delayed the aggregation of AtxQ78 (Figures 2A and 2B). The *C. elegans* NAC homolog also prevented AtxQ78 aggregation but was slightly less effective than the human isoform (Figure S2A).

Next, we mapped the PolyQ substrate binding site in NAC using a crosslinking and mass spectrometry (MS) approach. We used full-length AtxQ78 as our PolyQ model substrate for crosslinking to NAC for several reasons. First, AtxQ78 exhibits lower aggregation propensity than mHttQ51 or PolyQ51, allowing for crosslinking without concern for increasing the rate of the aggregation reaction. Second, the AtxQ78 construct does not require use of a solubilizing tag, avoiding the presence of additional factors during the crosslinking reaction. Third, while NAC may directly interact with the PolyQ region, glutamine does not contain any optimal functional groups for chemical crosslinking. However, AtxQ78 has many lysine residues, including several directly up-stream of the polyglutamine region, facilitating chemical crosslinking with amine-reactive crosslinkers (Figure S2B). Thus, crosslinks that occur within NAC to AtxQ78 regions adjacent to the polyglutamine tract may reflect the direct interaction between NAC and the PolyQ region, which we observed *in vitro* (Figures 1C and 1D). We incubated AtxQ78 with human NAC and used the amine-reactive homobifunctional crosslinker BS^3 to trap transient chaperone interactions. Crosslinked NAC-AtxQ78 complexes visible on Coomassie-stained gels (Figure S2C) were excised, and crosslinked peptides were identified by LC-MS using StavroX (Götze et al., 2012). Strikingly, 11 out of 18 identified intermolecular crosslinks were to the C-terminal region of AtxQ78 close to the expanded PolyQ stretch (Figure 2C, Table S1). These data suggest that NAC acts by binding at, or close to, the PolyQ tract to suppress aggregation of AtxQ78, which agrees with the observed NAC effect on the pure PolyQ51 substrate (Figures 1C and 1D). Interestingly, NAC predominantly crosslinked to AtxQ78 via the N-terminal regions of αNAC and βNAC (Figure 2C, Table S1), suggesting that a crucial PolyQ binding site is located in these domains. However, single crosslinks were also identified to the NAC domains, the UBA domain of αNAC, and to the C-terminal domain of βNAC.

The Ribosome-Binding Domain of NAC Exerts Chaperone Activity

Our data show that NAC exhibits direct chaperone activity toward diverse PolyQ substrates. Previous crosslinking data (Martin et al., 2018; Wiedmann et al., 1994) and our AtxQ78-NAC crosslinking-MS analysis indicate that NAC may interact with protein clients via both subunits. However, the specific substrate-binding site(s) of NAC critical for its chaperone function are unknown. To answer this, we took a mutational approach based on the evolutionarily conserved regions of NAC including the NAC dimerization domains, the C-terminal UBA domain of αNAC, and the N-terminal ribosome-binding domain of βNAC harboring a conserved ribosome-binding motif (RRKxxKK) (Figure 3A). First, we asked which of these conserved domains may be crucial for preventing PolyQ aggregation *in vivo*. We generated three *C. elegans* strains overexpressing mutant NAC constructs under the control of the *myo-3* promoter in the background of the PolyQ35::YFP strain. These included two deletion mutants lacking either the conserved αNAC UBA domain (ΔUBA-NAC) or the N-terminal βNAC domain (ΔNβ-NAC), as well as a mutation in the conserved ribosome-binding motif in the N terminus of βNAC (^{29}RRK/AAA^{31}-NAC) (Figure 3A), the latter of which abolished ribosome-binding of NAC *in vivo* (Figure S3A). All the NAC mutants expressed in *C. elegans* were stable and the expression levels were comparable to that of the overexpressed wild-type NAC complex (see FLAG immunoblot in Figures 3D and S3B). We assessed PolyQ35::YFP aggregation in these animals on day 3 of adulthood by fluorescence microscopy as well as SDD-AGE. We observed that both the ΔUBA-NAC and the RRK/AAA-NAC mutants suppressed PolyQ35::YFP

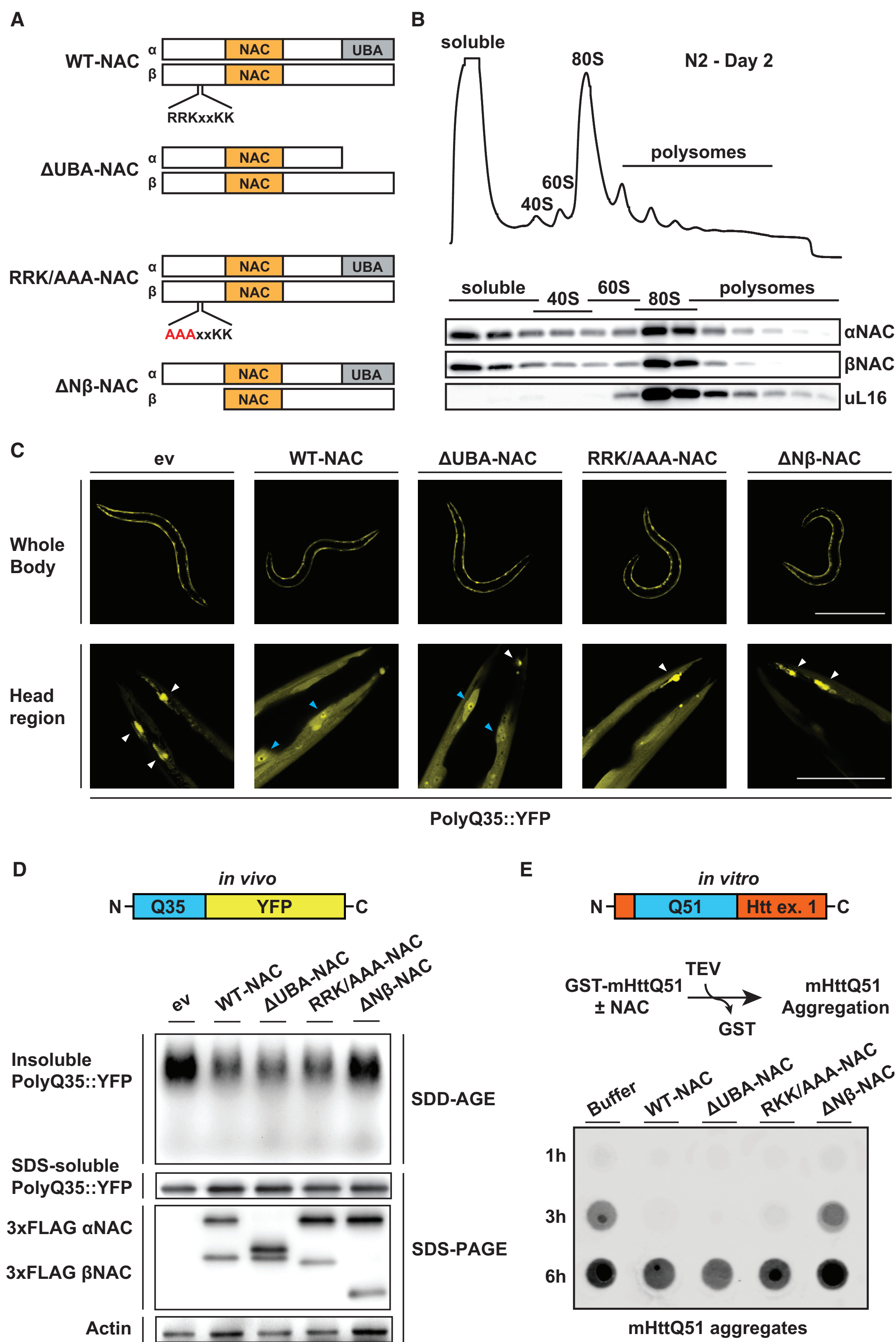

(legend on next page)

aggregation similarly to WT-NAC, indicated by the increased diffuse PolyQ35::YFP signal in the head region of these animals in comparison to control worms (ev) in which the majority of the PolyQ35::YFP is aggregated in puncta (Figure 3C). This correlated well with the levels of aggregated PolyQ35::YFP detected by SDD-AGE (Figure 3D). Thus, neither the UBA domain nor ribosome-association of NAC is required to suppress PolyQ35::YFP aggregation. The latter finding suggests that NAC may serve additional chaperone functions off the ribosome in *C. elegans.* These data were intriguing because analysis of NAC distribution in yeast shows it is almost exclusively associated with ribosomes (Raue et al., 2007). However, polysome profile analysis of NAC distribution in both *C. elegans* and human cells showed that a large fraction of NAC was not associated with ribosomes (Figures 3B and S3C), suggesting that NAC may also exert a post-translational chaperone function *in vivo*. The finding of a large pool of non-ribosome associated NAC under steady-state conditions in *C. elegans* and human cells together with the observed aggregation suppression activity of a NAC variant that does not bind to ribosomes both support the idea of off-ribosomal chaperone functions for NAC in the cytosol.

Strikingly, deletion of the N-terminal domain of βNAC abrogated the ability of NAC to suppress PolyQ35::YFP aggregation (Figures 3C, 3D, and S3B), indicating that this region contains an essential interaction site for PolyQ tracts, which is consistent with our AtxQ78-NAC crosslinking-MS data (Figure 2C). To address this possibility directly, we tested the ability of the different NAC mutants to suppress mHttQ51 aggregation *in vitro*, using purified components. Consistent with the *in vivo* results, addition of purified ΔUBA- or RRK/AAA-NAC delayed mHttQ51 aggregation similar to WT-NAC, whereas ΔNβ-NAC lost the ability to suppress aggregation (Figure 3E). In sum, the crosslinking data combined with the *in vitro* and *in vivo* PolyQ aggregation analyses strongly suggest that the N-terminal domain of βNAC contains a crucial PolyQ substrate-binding site. Importantly, our data also imply that NAC suppression of pathogenic PolyQ aggregation via this domain can occur in a ribosome-independent manner.

NAC Exerts Broad-Spectrum Chaperone Activity

Next, we investigated whether the identified NAC aggregation suppression activity involving N-βNAC is PolyQ specific or reflects a broad-spectrum chaperone activity. As a non-PolyQ model substrate, we used chemically denatured firefly luciferase that is known to rely on molecular chaperones to become refolded and luminesce (Schröder et al., 1993). Indeed, we found that luciferase activity after denaturation with guanidine-HCl (GdmCl) was restored after addition of an ATP-driven Hsp70/Hsp40 folding chaperone system (Figure S4A, green curve). Interestingly, we found that purified human NAC alone had no effect on luciferase refolding (Figure S4A, red curve) and did not enhance luciferase refolding upon addition to the Hsp70/Hsp40 system (Figure S4A, gray curve). However, when NAC was added to chemically denatured luciferase first, subsequent refolding by the Hsp70/Hsp40 system was strongly enhanced over levels of just Hsp70/Hsp40 refolding (Figure 4A, red versus green curve). A molar equivalent control protein of similar size, GFP, showed no enhancing effect (Figure S4B, black curve). Similar results were obtained with *C. elegans* NAC (Figure S4C, pink curve). That NAC was only effective in the initial stages of luciferase refolding was strikingly similar to the necessity of NAC to be involved in the earlier stages to suppress aggregation of mHttQ51 (Figure S1C). Thus, NAC exerts a general holdase chaperone function and maintains unfolded luciferase or pathogenic aggregation substrates in a soluble and refolding competent state. Importantly, we found that the activity of ΔNβ-NAC was significantly reduced compared to WT-NAC (Figure 4A, yellow curve). Thus, the same domain crucial to prevent PolyQ aggregation is also necessary to hold luciferase in a refolding competent state. However, in contrast to the PolyQ substrates, ΔNβ-NAC still exerted residual chaperone activity toward denatured luciferase, suggesting that NAC contains additional unidentified chaperone domains that can bind luciferase, a protein with higher sequence complexity than PolyQ-expanded Htt or AtxQ78.

We further investigated NAC activity on luciferase refolding *in vivo* using a *C. elegans* strain expressing a structurally destabilized version of luciferase fused to EGFP (FlucDM-EGFP) in muscle cells (Gupta et al., 2011). This protein is soluble at moderate temperature but aggregates upon heat stress. After heat shock (1 h, 33°C) of worms, FlucDM-EGFP formed large punctate aggregates that were still evident in control animals after 24 h recovery at 20°C (Figure 4B, "ev"). Overexpression of wild-type NAC in these worms allowed FlucDM-EGFP aggregation to fully revert back to diffuse GFP signal within the 24 h recovery phase (Figure 4B, "WT-NAC"), showing that NAC promotes *in vivo* refolding of luciferase, consistent with the *in vitro* findings (Figure 4A). Moreover, overexpression of ΔNβ-NAC was inefficient to revert heat-shock-induced FlucDM-EGFP aggregates back to the diffuse, soluble form after the 24 h

Figure 3. The Ribosome-Binding Domain of NAC Exerts Chaperone Activity

(A) Schematics showing the different heterodimeric NAC variants (α and β subunit) investigated in (C)–(E). Conserved domains (NAC and UBA) as well as the conserved ribosome-binding motif (RRKxxKK) in the β-subunit are highlighted.

(B) Sucrose density gradient analysis in wild-type N2 worms on day 2 of adulthood. Upper image shows polysome gradient profile (absorbance at 254 nm). Immunoblot images below show the distribution of NAC (α- and β-subunit) throughout the gradient. uL16 served as a ribosomal marker.

(C) Fluorescence microscope images of PolyQ35::YFP worms overexpressing WT-NAC or different mutant NAC versions shown in (A). Images were taken at day 3 of adulthood. Scalebar, 500 μm (upper row) and 50 μm (lower row). PolyQ35::YFP aggregates and cell nuclei are indicated by white and blue arrowheads, respectively. ev, empty vector.

(D) SDD-AGE immunoblot showing the PolyQ35::YFP aggregation in animals as in (C). Total levels of SDS-soluble PolyQ35::YFP and FLAG-tagged NAC variants were assessed by SDS-PAGE immunoblot analysis. Actin served as loading control.

(E) *In vitro* filter trap aggregation assay of mutant Huntingtin (mHttQ51) incubated with 5× molar excess of indicated NAC variants. Aggregation of GST-mHttQ51 was initiated by cleavage of the GST tag using the TEV protease. SDS-insoluble aggregates were detected with an S-tag antibody.

See also Figure S3.

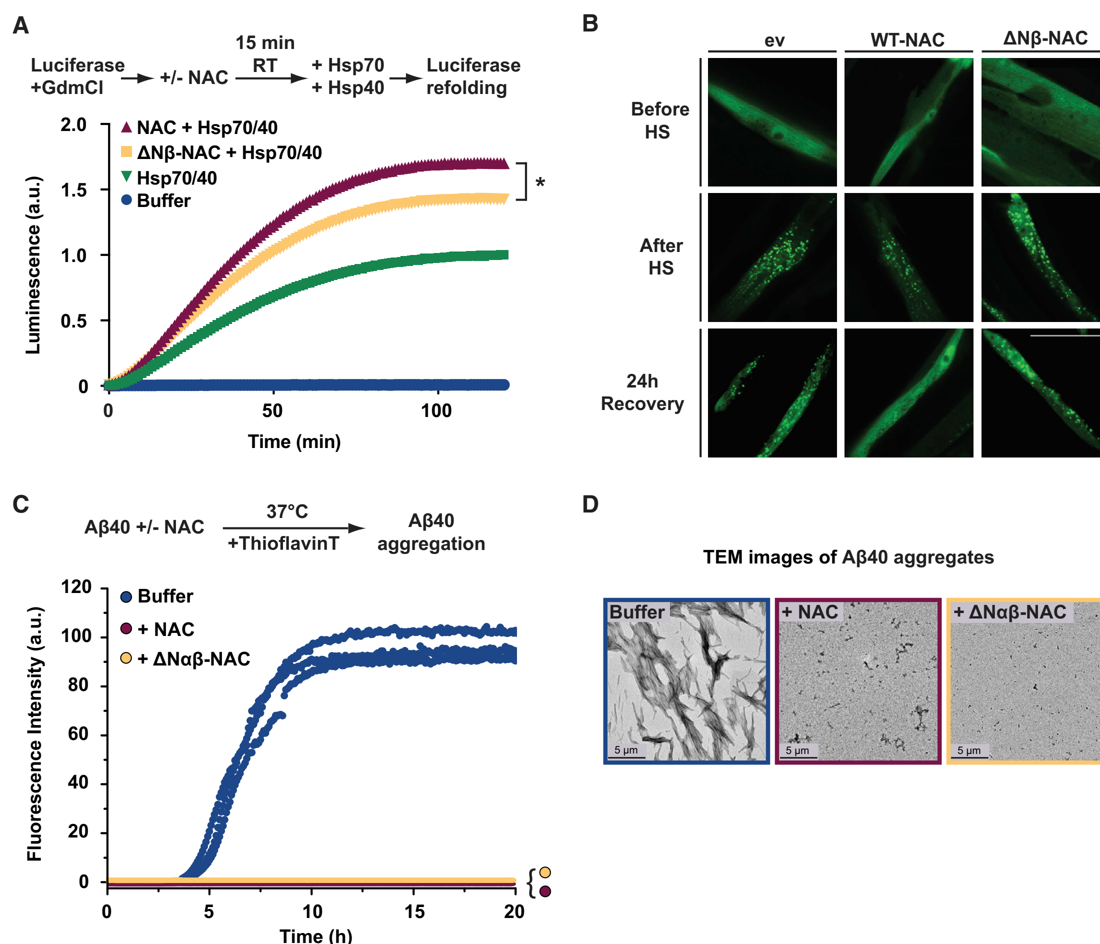

Figure 4. NAC Exerts Broad-Spectrum Chaperone Activity

(A) *In vitro* chaperone refolding assays using guanidine-HCl (GdmCl)-denatured luciferase as substrate. Luciferase (0.02 μM) was preincubated with indicated NAC variants in a 1:1 molar ratio for 15 min at room temperature, and refolding was initiated by adding an Hsp70/Hsp40 chaperone system (3.2 μM/0.8 μM). Luciferase reactivation was analyzed by luminescence recording over 2 h at RT using luciferin as a substrate. Statistical significance was calculated by one-way ANOVA and Tukey post hoc test. a.u., arbitrary units. *$p < 0.05$ (n = 3).

(B) Fluorescence microscope images of *C. elegans* worms expressing a destabilized variant of firefly luciferase fused to EGFP (FlucDM-EGFP) and indicated NAC variants (FLAG-tagged α and βNAC) in muscle cells. Images were taken before heat shock (HS, 1 h at 33°C), directly after HS, and after 24 h recovery at 20°C. Scale bar, 20 μm. ev, empty vector.

(C) Kinetic aggregation assays of Aβ40 (32 μM, blue) incubated with an equimolar concentration of WT-NAC (red) or ΔNαβ-NAC (yellow) measured using ThioflavinT fluorescence. a.u., arbitrary units.

(D) Negative stain transmission electron micrographs of the reaction endpoint (at 20 h) for each sample shown in (C). Scale bar, 5 μm.

See also Figure S4 and Table S2.

recovery period (Figure 4B, "ΔNβ-NAC," and Figure S4D). Thus, efficient luciferase refolding depends on N-βNAC, *in vitro* and *in vivo*. Overall, these data corroborate that the N terminus of βNAC represents a central chaperone domain of NAC for luciferase as well as for PolyQ substrates.

Next, we investigated whether NAC suppresses aggregation of the Alzheimer's disease-related Aβ40 peptide which, in contrast to PolyQ, has a more complex sequence, including regions more hydrophobic in character. Aβ40 aggregation was recorded over time *in vitro* using Thioflavin T (ThT) fluorescence as a readout for amyloid fibril formation. In the absence of NAC, we observed a rapid increase of ThT fluorescence, indicating Aβ40 aggregation (Figure 4C, "Buffer"), and electron microscope analysis confirmed formation of aggregates with fibrillar structure (Figure 4D). Remarkably, equimolar addition of purified human NAC completely suppressed Aβ40 aggregation and fibril formation (Figures 4C and 4D). In addition, ΔUBA- and RRK/AAA-NAC mutants also fully suppressed Aβ40 aggregation (Figure S4E). However, in contrast to the PolyQ substrates and luciferase, the N-terminal βNAC domain was dispensable for preventing aggregation of the highly hydrophobic Aβ40 substrate. Though crosslinking-MS analyses indicated an interaction of Aβ40 with the N-terminal domains of NAC similar to AtxQ78 (Figures S4F and S4G), NAC mutants lacking the βNAC N terminus (ΔNβ-NAC) or the N termini of both subunits (ΔNαβ-NAC) were fully active in suppressing Aβ40 aggregation comparably to WT-NAC

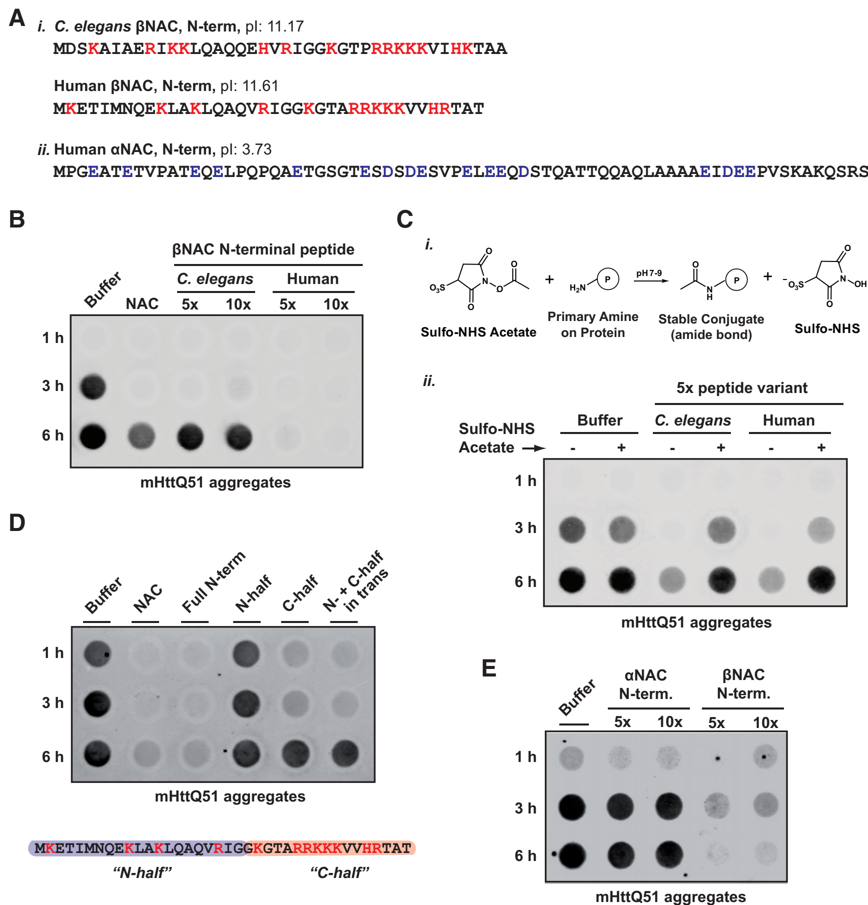

Figure 5. Functional Characterization of the N-Terminal βNAC Chaperone Domain

(A) (*i*) Peptide sequences of N-termini of βNAC from *C. elegans* and humans. Positively charged residues are highlighted in red. Both peptides exhibit a considerably high isoelectric point (pI). (*ii*) N-terminal peptide sequence of human αNAC exhibiting in contrast to βNAC peptides a low pI. Negatively charged residues are highlighted in blue.

(B) *In vitro* filter trap aggregation assay of mutant Huntingtin (mHttQ51) incubated with 5× or 10× molar excess of βNAC peptides shown in (A) or full-length NAC protein.

(C) (*i*) Chemical reaction scheme showing acylation of primary amines by Sulfo-NHS-acetate used to neutralize the positive charge in lysine residues of βNAC peptides shown in (A). (*ii*) *In vitro* filter trap aggregation assay of mutant Huntingtin (mHttQ51) incubated with 5× molar excess of peptides shown in (A) with and without Sulfo-NHS-acetate labeling.

(D) *In vitro* filter trap aggregation assay of mutant Huntingtin (mHttQ51) incubated with 5× molar excess of full-length NAC protein (NAC), full N-terminal βNAC peptide (Full N-term), or the N- and C-half of the peptide as indicated in the schematic below (N- and C-half highlighted in blue and red, respectively).

(E) *In vitro* filter trap aggregation assay of mutant Huntingtin (mHttQ51) incubated with 5× or 10× molar excess of human α- or βNAC peptides shown in (A).

See also Figure S5.

(Figures 4C, 4D, and S4E). Thus, NAC likely contains other important substrate interaction sites that may specifically bind hydrophobic segments in substrates such as Aβ40 and luciferase.

In sum, these data show that NAC is able to chaperone diverse substrates with different structural and physicochemical properties, corroborating a broad-spectrum chaperone function of NAC. Moreover, our data reveal that the N-terminal βNAC domain confers substrate-specific chaperone function.

Functional Characterization of the N-Terminal βNAC Chaperone Domain

Our data show that the N-terminal domain of βNAC not only confers ribosome-binding but also has chaperone activity, preventing the aggregation of PolyQ proteins and promoting refolding of firefly luciferase. This small domain (~40 aa) is characterized by a high positive net charge, in particular at its C-terminal half, which is predicted to be unstructured (Figure 5A). To gain more insight into the chaperone activity of this domain, we utilized synthetic peptides corresponding to the N-terminal region of βNAC from human and *C. elegans* in *in vitro* aggregation assays. We observed that these N-βNAC peptides alone were sufficient to suppress aggregation of mHttQ51 (Figure 5B). Similar aggregation suppression results were obtained when using the pure PolyQ51 substrate (Figure S5A), indicating a direct interaction of the N-βNAC peptides with the polyglutamine stretch.

The most obvious characteristic of the N-βNAC peptides is the high positive net charge (Figure 5A). In addition to hydrophobic contacts, electrostatic interactions mediated via highly charged regions in chaperones are emerging to play an important role in client binding (He et al., 2016; Horowitz et al., 2016; Joachimiak et al., 2014). Thus, we asked whether the positively charged residues contribute to the ability of these peptides to suppress PolyQ aggregation. To address this, we acylated primary amines in lysine residues of the peptides using Sulfo-NHS-acetate in order to neutralize the positive charge (Figures 5Ci and S5B). Interestingly, we observed that upon labeling the lysine residues, the peptides significantly lost their ability to suppress mHttQ51 aggregation (Figure 5C*ii*). Thus, the positively charged residues in N-βNAC are critical for its chaperone activity. To investigate this in more detail, we split the human peptide into two halves, resulting in an N-terminal peptide containing a predicted conserved helical element with several hydrophobic residues and a C-terminal peptide encompassing most of the conserved positively charged residues (Figure 5D). Remarkably, the C-terminal half of N-βNAC was alone able to suppress mHttQ51 aggregation, whereas the N-terminal half showed no effect (Figure 5D). This finding corroborates that the primary PolyQ binding

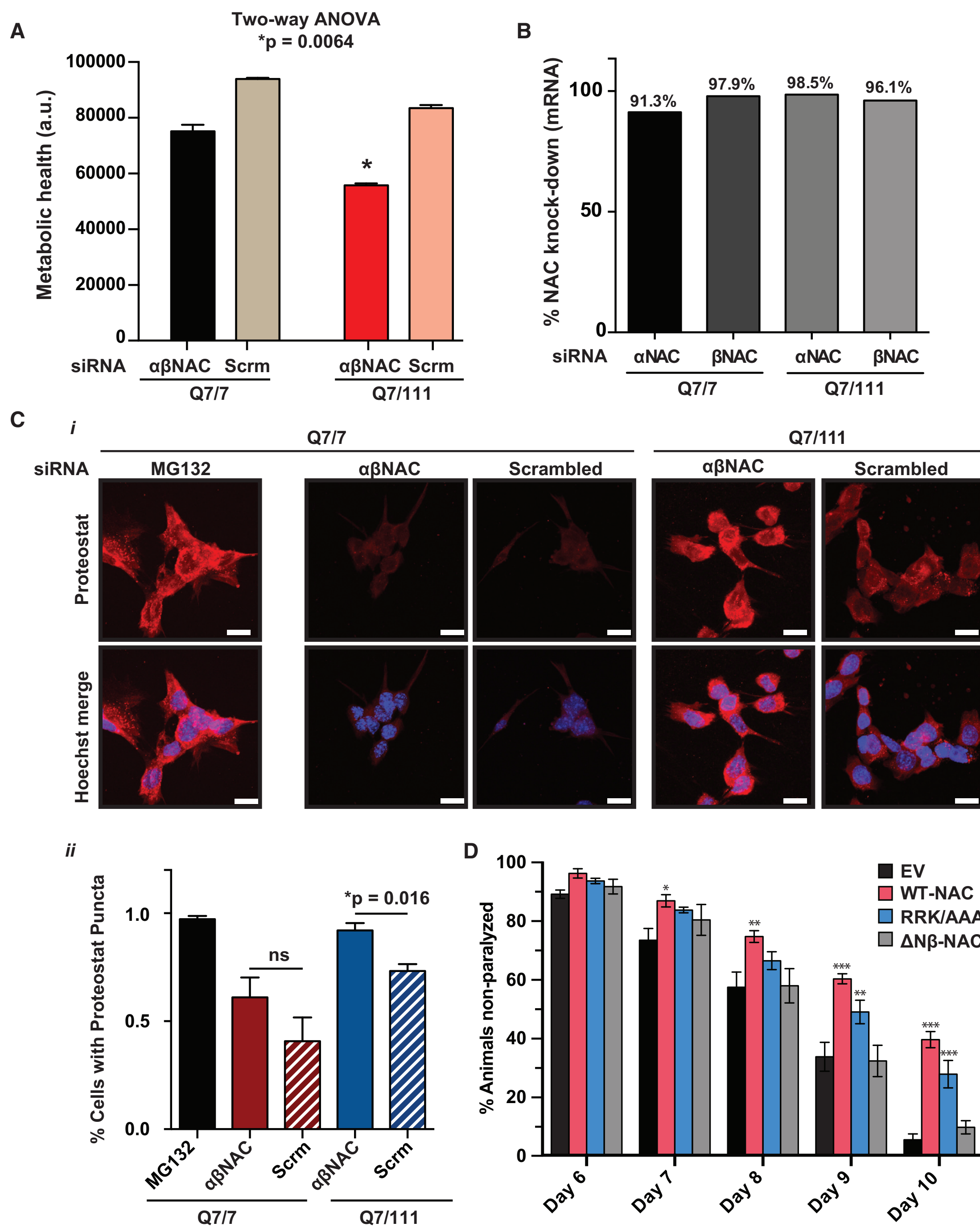

Figure 6. NAC Suppresses Toxicity of PolyQ Proteins

(A) Viability of mouse striatal neurons either homozygous for wild-type Huntingtin (Q7/7) or heterozygous for mutant Huntingtin (Q7/111). Metabolically active cells were quantified by measuring ATP levels using the Cell Titer Glo assay after 3-day treatment with siRNAs targeting both NAC subunits. Scrambled (Scrm) siRNA sequences were used as control. Data are represented as mean ± SEM. Statistical significance was determined by two-way ANOVA. Data are representative of at least 5 independent biological replicates. a.u., arbitrary units.

(B) Quantification of α/βNAC knockdown by qPCR in the mouse striatal cell lines Q7/7 and Q7/111. Actin was used as a housekeeping gene control. Knockdown of α/βNAC was compared to the scrambled control condition.

(C) (*i*) Homozygous wild-type (Q7/7) and heterozygous mutant (Q7/111) Huntingtin cells were treated with NAC siRNA or a scrambled control (Scrm) for 3 days. Fluorescence microscope images show cells stained with Proteostat fluorescent dye to assess protein aggregation. Cells treated with the proteasome inhibitor MG132 (5 μM, 6 h) were used as positive aggregation control. Scale bar, 15 μm. Hoechst was used to label nuclei of cells. (*ii*) Diagram shows the ratio of Proteostat fluorescence to Hoechst fluorescence in cells shown as in (*i*). Data are represented as mean ± SEM (n = 3).

(legend continued on next page)

site is located in the positively charged stretch of the peptide. Although very potent, the C-terminal peptide was not as completely effective as the full-length peptide or the full-length NAC chaperone in suppressing mHttQ51 aggregation (Figure 5D). This suggests that additional regions in the N-βNAC peptide contribute to the chaperone activity. Of note, mixing the N-half peptide and the C-half peptides did not increase the aggregation suppression ability over the C-half peptide alone (Figure 5D). Thus, full function is only obtained by a cooperative activity that relies on the entire N-βNAC.

We also investigated the activity of the N terminus of the αNAC subunit, which is also highly charged, albeit with a net negative charge (Figure 5A). This domain is thought to be flexible, similar to the βNAC N-terminal region, and our AtxQ78-NAC crosslinking data indicated an interaction with the mutant PolyQ domain (Figure 2C). However, we found that N-αNAC peptides either added alone or in combination with the N-βNAC peptides had no effect on mHttQ51 aggregation (Figures 5E and S5C), even at 10× molar excess over the mHttQ51 substrate, underscoring the specificity of the aggregation suppression effect by the positively charged βNAC N-terminal domain.

NAC Suppresses Toxicity of PolyQ Proteins in Neuronal Cell Lines and Animals

Next, we investigated the relevance of NAC to mutant Huntingtin toxicity in neuronal cells. Here, we used a knockin mouse striatal cell line heterozygous for a 111-glutamine residue repeat mutation in the full-length Huntingtin protein (HttQ7/111), which is a well-established cell line to model Huntington's disease pathology (Trettel et al., 2000). We compared the phenotype of this mutant Huntingtin cell line with that of a striatal mouse cell line homozygous for the wild-type Huntingtin allele (HttQ7/7). First, we assessed how knockdown of NAC would affect viability of mHtt-expressing cells. We depleted both NAC subunits by siRNA, and after 72 h determined the number of metabolically active cells by measuring ATP levels using the Cell Titer Glo assay. While knockdown of NAC decreased health of both cell lines, the mHtt-expressing HttQ7/111 cells were significantly more sensitive toward NAC depletion (Figure 6A). Knockdown efficiency of αNAC and βNAC was comparable in two Htt cell lines (Figures 6B and S6). Thus, while NAC generally promotes striatal neuron health, NAC is especially critical to maintain metabolic health of neurons expressing mutant, aggregation-prone Huntingtin. To address whether ribosome-binding of NAC was necessary for this protective function, we tried to overexpress different NAC variants in striatal cells. However, this was not possible, so it remains unclear whether suppression of Htt toxicity in neurons by NAC results from its co- and/or post-translational function.

To understand the specific need for NAC in maintaining metabolic function of mHtt-expressing striatal neurons, we asked whether NAC was especially crucial for neuronal protein homeostasis in the presence of mutant Huntingtin. Therefore, we analyzed the protein aggregation burden in both wild-type (HttQ7/7) and mutant Htt-expressing cells (HttQ7/111) upon silencing of NAC. Protein aggregation was assessed using the Proteostat dye, which recognizes aggregates from a broad range of protein substrates (Shen et al., 2011). We observed that in wild-type cells, knockdown of NAC had a negligible effect on protein aggregation, whereas protein aggregates strongly accumulated in the mHtt-expressing cells (Figure 6C). Thus, NAC is essential to counteract the increased burden on the protein homeostasis machinery provoked by mHtt expression, demonstrating the essential, physiologically protective role NAC plays in maintaining protein homeostasis.

Finally, because protein aggregation has been tightly linked to age-associated organismal degeneration (Sala et al., 2017), we asked whether NAC is also essential for organismal fitness and healthy aging. We overexpressed wild-type NAC and mutant ΔNβ-NAC in *C. elegans* expressing the aggregation-prone PolyQ35::YFP and measured age-associated paralysis (Cohen et al., 2006; Morley et al., 2002). We found that overexpressing wild-type NAC significantly improves motility of PolyQ35::YFP-expressing worms during aging (Figure 6D), suggesting that overexpression of NAC alone can improve protein homeostasis and organismal health. In addition, we found that this improvement in motility strictly depends on the presence of the N terminus of βNAC (Figure 6D), highlighting the importance of this domain in maintaining protein homeostasis in aging. Importantly, the protective activity of N-βNAC is mostly independent from its ribosome-binding role as overexpression of the ribosome-binding deficient RRK/AAA-NAC variant still improved motility during aging, albeit less effective than WT-NAC (Figure 6D). Thus, ribosome-binding of NAC contributes but is not essential under these conditions per se for improving protein homeostasis and organismal health in aging. Overall, these data show the tight linkage between cellular and organismal proteostatic health and the chaperone role of NAC as mediated by the N terminus of the βNAC subunit.

DISCUSSION

Our data show that the same domain of NAC critical for ribosome-binding also exerts chaperone activity. Thus, N-βNAC has a dual role and may serve chaperone functions on and off the ribosome. NAC may contact nascent substrates via N-βNAC to promote co-translational folding, and, likewise, this domain binds misfolded cytosolic proteins post-translationally to prevent aggregation. Indeed, NAC exists in an equilibrium between a ribosome-bound and unbound state under steady-state conditions with a large non-ribosomal population. Our data also clearly show that the chaperone function of NAC is not restricted to co-translational *de novo* protein synthesis as revealed by the ribosome-independent aggregation suppression effect of NAC on PolyQ proteins *in vivo* and *in vitro*. We suggest a model in which the canonical activity of NAC in co-translational protein

(D) Diagram shows the percentage of non-paralyzed PolyQ35::YFP *C. elegans* worms overexpressing either wild-type NAC (WT-NAC), ribosome-binding deficient NAC (RRK/AAA), or NAC lacking the N-terminal region of βNAC (ΔNβ-NAC) between days 6 and 10 of adulthood. Data are represented as mean ± SEM (n = 3). Statistical significance was calculated by Student's t test. **/***$p < 0.01/0.001$ versus WT-NAC. EV, empty vector.
See also Figure S6.

transport and folding (del Alamo et al., 2011; Gamerdinger et al., 2015) is complemented by its off-ribosomal chaperone activity to prevent aggregation of misfolded cytosolic protein species. Whether ribosome-associated NAC also actively dissociates from the ribosome during protein stress to chaperone aggregation-prone substrates is an attractive hypothesis and remains to be further explored. Previous data suggested an elegant mechanism for how NAC binding to misfolded protein species might be coupled to ribosome detachment under high proteotoxic stress (Kirstein-Miles et al., 2013). This stress-induced ribosome dissociation of NAC could be mediated by other chaperone cofactors activated by the presence of protein aggregation or by bulk association upon accumulation of protein aggregates.

NAC has broad chaperone activity toward distinct types of substrates, including PolyQ, Aβ40, and luciferase. The type of misfolded or unfolded domain that NAC recognizes remains unclear. We find that NAC is most effective in the early stages of misfolding of aggregation-prone pathogenic proteins (Figure S1D). This suggests that NAC may act as a holdase chaperone that recognizes a misfolded intermediate appearing early in the aggregation reaction. NAC may then prepare these early-aggregation species substrates for further manipulation by other chaperones as demonstrated for luciferase in this study (Figure 4A) or sequester aggregation-prone domains critical in the early stages of oligomerization. It is tempting to envision a similar activity for NAC when acting on nascent polypeptides. The affinity of NAC for different misfolded protein domains remains to be determined, and affinity may well depend both on the sequence and conformational properties of the client, as is observed for other ATP-independent chaperones (Saio et al., 2014; Stull et al., 2016). Our *in vitro* experiments demonstrate a concentration dependence of NAC suppression of PolyQ aggregation (Figure S1B), with higher molar excess of NAC over the client resulting in greater aggregation suppression. Such an observation is consistent with findings on other ATP-independent chaperones that bind their substrates weakly, such that an excess of chaperone is required to enable chaperone binding to compete effectively with aggregation. Importantly, NAC is an abundant protein *in vivo* and is at least stoichiometric with the ribosome (Raue et al., 2007), which would enable effective chaperoning even for weakly binding clients that are highly aggregation-prone. Thus, even if only a small percentage of NAC associates with misfolded Htt substrates at any given time, rapid binding and release, combined with potential remodeling of the protein client in the bound state, could also enhance folding and decrease the probability of aggregation. This would enable these proteins to remain soluble so that they can fold spontaneously or be bound by other chaperones that complete folding or target misfolded proteins to degradation pathways (Balchin et al., 2016; Saibil, 2013).

The discovery that just the positively charged N terminus of βNAC is sufficient to potently suppress mutant PolyQ aggregation *in vitro*, as well as necessary to delay age-associated paralysis in *C. elegans*, has important implications for a general binding mechanism of chaperones to mutant PolyQ substrates. While the PolyQ itself is uncharged, its polarity can still take part in weak electrostatic interactions with a charged surface like the βNAC N terminus. Indeed, hydrophilic regions have been associated with chaperone-substrate recognition patterns in addition to the more canonical hydrophobic regions. For example, the TRiC chaperonin, a potent suppressor of mHtt aggregation and toxicity, contains bipartite hydrophilic and hydrophobic substrate recognition sites (Joachimiak et al., 2014). It has been proposed that both of these domains may recognize either hydrophobic or hydrophilic regions of mHtt to mediate suppression of aggregation (Joachimiak et al., 2014; Tam et al., 2006, 2009). DNAJB6 suppresses aggregation of expanded PolyQ tracts through a serine/threonine-rich domain, which disrupts formation of stabilizing hydrogen bonding among the PolyQ residues (Kakkar et al., 2016). It is intriguing that there seems to be specificity with respect to charge: while the N-terminal region of the αNAC subunit is also highly charged, it is net negatively charged and has little to no effect on Htt aggregation (Figure 5E). Thus, it seems that an overall net positive charge is specific for suppression of PolyQ aggregation, but reasons why are still unclear.

Finally, the ability of the βNAC N-terminal peptide to suppress aggregation makes this an important sequence for possible therapeutic development. How NAC is able to recognize different misfolded substrates is an intriguing question for further exploration. A strong overexpression of full-length NAC is poorly tolerated on the organismal level (Gamerdinger et al., 2015), potentially due to its binding mode at the ribosomal exit site that is competitive with other essential protein biogenesis factors. This restricts a potential therapeutic intervention strategy that aims to increase NAC expression levels to combat PolyQ diseases. However, delivery or overexpression of just the N-terminal peptide, which is sufficient to suppress PolyQ aggregation, may be much better tolerated in an organism and thus an effective an anti-aggregation therapeutic strategy. In sum, this study provides a detailed understanding of a chaperone activity of NAC off the ribosome and highlights a substrate recognition mechanism that is based on positive charges which provides a possible avenue for a peptide-based therapeutics approach in Huntington's disease and related PolyQ disorders.

STAR★METHODS

Detailed methods are provided in the online version of this paper and include the following:

- KEY RESOURCES TABLE
- CONTACT FOR REAGENT AND RESOURCE SHARING
- EXPERIMENTAL MODEL AND SUBJECT DETAILS
  - Cell lines
  - *C. elegans* strains
- METHOD DETAILS
  - Protein purification
  - *In vitro* aggregation assays
  - Thioflavin T fluorescence assay
  - Transmission electron microscopy
  - Cell viability assays and real-time PCR
  - Fluorescence microscopy of cells
  - Polysome analysis in human cells
  - Sulfo-NHS peptide labeling
  - Chemical crosslinking and mass spectrometry

- ○ Luciferase refolding assay
- ○ *C. elegans* transformation
- ○ Synchronization of *C. elegans*
- ○ Fluorescence microscopy of worms
- ○ SDD-AGE
- ○ Polysome analysis of worms
- ○ Paralysis assay
- ○ Immunoblot analysis in *C. elegans*
- ● QUANTIFICATION AND STATISTICAL ANALYSIS
  - ○ Experimental procedure
  - ○ Statistics
- ● DATA AND SOFTWARE AVAILABILITY

SUPPLEMENTAL INFORMATION

Supplemental Information can be found online at https://doi.org/10.1016/j.molcel.2019.03.012.

ACKNOWLEDGMENTS

We thank Christina Schlatterer for preparing the graphical abstract. We thank the members of our research groups for valuable support and discussion of the manuscript, Sandra Macedo-Ribeiro for collaborations on Atx-3, and Alison Ashcroft and James Ault for collaborations on biological MS. This work was supported by research grants from the German Science Foundation (DFG; SFB969; A01 and A07) to E.D. and M.G., from Human Frontier in Science (HFSP) to S.E.R., E.D., and J.F., and by a guest-professorship for J.F. by the State Baden-Württemberg. E.M.M. was supported by HFSP (RGP0025) and the Wellcome Trust Institutional Strategic Fund (RGP0025/2012). S.E.R. acknowledges the Wellcome Trust (09154/Z/15/Z) and the European Research Council (ERC) under European Union's Seventh Framework Programme (FP7/2007–2013) ERC grant agreement no. 322408 for funding. We also thank the BBSRC for funding A.N.C., P.D.K., and K.L.S. (BB/P000037/1, BB/J014443/1 and BB/K01451X/1, respectively) and the Wellcome Trust and BBSRC for funding the Astbury Centre's mass spectrometry equipment (BB/M012573/11 and 208385/Z/17/Z). We are thankful for NIH grants GM056433 and NS092525 to J.F.

AUTHOR CONTRIBUTIONS

Conceptualization, M.G., K.S., S.E.R., J.F., and E.D.; Investigation, K.G., R.C., E.M.M., N.S., P.D.K., R.S., A.N.C., K.L.S., L.L., A.B., K.S., and M.G.; Writing – Original Draft, M.G. and K.S.; Writing – Review & Editing, S.E.R., J.F., and E.D.; Funding Acquisition, M.G., S.E.R., J.F., and E.D.

DECLARATION OF INTERESTS

The authors declare no competing interests.

Received: September 7, 2018
Revised: January 22, 2019
Accepted: March 8, 2019
Published: April 11, 2019

REFERENCES

Balchin, D., Hayer-Hartl, M., and Hartl, F.U. (2016). In vivo aspects of protein folding and quality control. Science *353*, aac4354.

Brenner, S. (1974). The genetics of Caenorhabditis elegans. Genetics *77*, 71–94.

Cohen, E., Bieschke, J., Perciavalle, R.M., Kelly, J.W., and Dillin, A. (2006). Opposing activities protect against age-onset proteotoxicity. Science *313*, 1604–1610.

del Alamo, M., Hogan, D.J., Pechmann, S., Albanese, V., Brown, P.O., and Frydman, J. (2011). Defining the specificity of cotranslationally acting chaperones by systematic analysis of mRNAs associated with ribosome-nascent chain complexes. PLoS Biol. *9*, e1001100.

Duttler, S., Pechmann, S., and Frydman, J. (2013). Principles of cotranslational ubiquitination and quality control at the ribosome. Mol. Cell *50*, 379–393.

Frøkjaer-Jensen, C., Davis, M.W., Hopkins, C.E., Newman, B.J., Thummel, J.M., Olesen, S.P., Grunnet, M., and Jorgensen, E.M. (2008). Single-copy insertion of transgenes in Caenorhabditis elegans. Nat. Genet. *40*, 1375–1383.

Gamerdinger, M., Hanebuth, M.A., Frickey, T., and Deuerling, E. (2015). The principle of antagonism ensures protein targeting specificity at the endoplasmic reticulum. Science *348*, 201–207.

Götze, M., Pettelkau, J., Schaks, S., Bosse, K., Ihling, C.H., Krauth, F., Fritzsche, R., Kühn, U., and Sinz, A. (2012). StavroX–a software for analyzing crosslinked products in protein interaction studies. J. Am. Soc. Mass Spectrom. *23*, 76–87.

Gupta, R., Kasturi, P., Bracher, A., Loew, C., Zheng, M., Villella, A., Garza, D., Hartl, F.U., and Raychaudhuri, S. (2011). Firefly luciferase mutants as sensors of proteome stress. Nat. Methods *8*, 879–884.

Halfmann, R., and Lindquist, S. (2008). Screening for amyloid aggregation by Semi-Denaturing Detergent-Agarose Gel Electrophoresis. J. Vis. Exp. *17*, 838.

He, L., Sharpe, T., Mazur, A., and Hiller, S. (2016). A molecular mechanism of chaperone-client recognition. Sci. Adv. *2*, e1601625.

Horowitz, S., Salmon, L., Koldewey, P., Ahlstrom, L.S., Martin, R., Quan, S., Afonine, P.V., van den Bedem, H., Wang, L., Xu, Q., et al. (2016). Visualizing chaperone-assisted protein folding. Nat. Struct. Mol. Biol. *23*, 691–697.

Joachimiak, L.A., Walzthoeni, T., Liu, C.W., Aebersold, R., and Frydman, J. (2014). The structural basis of substrate recognition by the eukaryotic chaperonin TRiC/CCT. Cell *159*, 1042–1055.

Kakkar, V., Månsson, C., de Mattos, E.P., Bergink, S., van der Zwaag, M., van Waarde, M.A.W.H., Kloosterhuis, N.J., Melki, R., van Cruchten, R.T.P., Al-Karadaghi, S., et al. (2016). The S/T-rich motif in the DNAJB6 chaperone delays polyglutamine aggregation and the onset of disease in a mouse model. Mol. Cell *62*, 272–283.

Kim, Y.E., Hipp, M.S., Bracher, A., Hayer-Hartl, M., and Hartl, F.U. (2013). Molecular chaperone functions in protein folding and proteostasis. Annu. Rev. Biochem. *82*, 323–355.

Kirstein-Miles, J., Scior, A., Deuerling, E., and Morimoto, R.I. (2013). The nascent polypeptide-associated complex is a key regulator of proteostasis. EMBO J. *32*, 1451–1468.

Labbadia, J., and Morimoto, R.I. (2013). Huntington's disease: underlying molecular mechanisms and emerging concepts. Trends Biochem. Sci. *38*, 378–385.

Liu, Y., Hu, Y., Li, X., Niu, L., and Teng, M. (2010). The crystal structure of the human nascent polypeptide-associated complex domain reveals a nucleic acid-binding region on the NACA subunit. Biochemistry *49*, 2890–2896.

Martin, E.M., Jackson, M.P., Gamerdinger, M., Gense, K., Karamonos, T.K., Humes, J.R., Deuerling, E., Ashcroft, A.E., and Radford, S.E. (2018). Conformational flexibility within the nascent polypeptide-associated complex enables its interactions with structurally diverse client proteins. J. Biol. Chem. *293*, 8554–8568.

Matos, C.A., de Macedo-Ribeiro, S., and Carvalho, A.L. (2011). Polyglutamine diseases: the special case of ataxin-3 and Machado-Joseph disease. Prog. Neurobiol. *95*, 26–48.

Mello, C., and Fire, A. (1995). DNA transformation. Methods Cell Biol. *48*, 451–482.

Morley, J.F., Brignull, H.R., Weyers, J.J., and Morimoto, R.I. (2002). The threshold for polyglutamine-expansion protein aggregation and cellular toxicity is dynamic and influenced by aging in Caenorhabditis elegans. Proc. Natl. Acad. Sci. USA *99*, 10417–10422.

Ott, A.K., Locher, L., Koch, M., and Deuerling, E. (2015). Functional dissection of the nascent polypeptide-associated complex in saccharomyces cerevisiae. PLoS ONE *10*, e0143457.

Pech, M., Spreter, T., Beckmann, R., and Beatrix, B. (2010). Dual binding mode of the nascent polypeptide-associated complex reveals a novel universal adapter site on the ribosome. J. Biol. Chem. *285*, 19679–19687.

Pechmann, S., Willmund, F., and Frydman, J. (2013). The ribosome as a hub for protein quality control. Mol. Cell *49*, 411–421.

Preissler, S., and Deuerling, E. (2012). Ribosome-associated chaperones as key players in proteostasis. Trends Biochem. Sci. *37*, 274–283.

Raue, U., Oellerer, S., and Rospert, S. (2007). Association of protein biogenesis factors at the yeast ribosomal tunnel exit is affected by the translational status and nascent polypeptide sequence. J. Biol. Chem. *282*, 7809–7816.

Saibil, H. (2013). Chaperone machines for protein folding, unfolding and disaggregation. Nat. Rev. Mol. Cell Biol. *14*, 630–642.

Saio, T., Guan, X., Rossi, P., Economou, A., and Kalodimos, C.G. (2014). Structural basis for protein antiaggregation activity of the trigger factor chaperone. Science *344*, 1250494.

Sala, A.J., Bott, L.C., and Morimoto, R.I. (2017). Shaping proteostasis at the cellular, tissue, and organismal level. J. Cell Biol. *216*, 1231–1241.

Saunders, H.M., and Bottomley, S.P. (2009). Multi-domain misfolding: understanding the aggregation pathway of polyglutamine proteins. Protein Eng. Des. Sel. *22*, 447–451.

Scarff, C.A., Almeida, B., Fraga, J., Macedo-Ribeiro, S., Radford, S.E., and Ashcroft, A.E. (2015). Examination of Ataxin-3 (atx-3) aggregation by structural mass spectrometry techniques: a rationale for expedited aggregation upon polyglutamine (polyQ) expansion. Mol. Cell. Proteomics *14*, 1241–1253.

Schindelin, J., Arganda-Carreras, I., Frise, E., Kaynig, V., Longair, M., Pietzsch, T., Preibisch, S., Rueden, C., Saalfeld, S., Schmid, B., et al. (2012). Fiji: an open-source platform for biological-image analysis. Nat. Methods *9*, 676–682.

Schröder, H., Langer, T., Hartl, F.U., and Bukau, B. (1993). DnaK, DnaJ and GrpE form a cellular chaperone machinery capable of repairing heat-induced protein damage. EMBO J. *12*, 4137–4144.

Shen, D., Coleman, J., Chan, E., Nicholson, T.P., Dai, L., Sheppard, P.W., and Patton, W.F. (2011). Novel cell- and tissue-based assays for detecting misfolded and aggregated protein accumulation within aggresomes and inclusion bodies. Cell Biochem. Biophys. *60*, 173–185.

Stewart, K.L., Hughes, E., Yates, E.A., Middleton, D.A., and Radford, S.E. (2017). Molecular Origins of the Compatibility between Glycosaminoglycans and Aβ40 Amyloid Fibrils. J. Mol. Biol. *429*, 2449–2462.

Stull, F., Koldewey, P., Humes, J.R., Radford, S.E., and Bardwell, J.C.A. (2016). Substrate protein folds while it is bound to the ATP-independent chaperone Spy. Nat. Struct. Mol. Biol. *23*, 53–58.

Sun, L., Edelmann, F.T., Kaiser, C.J., Papsdorf, K., Gaiser, A.M., and Richter, K. (2012). The lid domain of Caenorhabditis elegans Hsc70 influences ATP turnover, cofactor binding and protein folding activity. PLoS ONE *7*, e33980.

Tam, S., Geller, R., Spiess, C., and Frydman, J. (2006). The chaperonin TRiC controls polyglutamine aggregation and toxicity through subunit-specific interactions. Nat. Cell Biol. *8*, 1155–1162.

Tam, S., Spiess, C., Auyeung, W., Joachimiak, L., Chen, B., Poirier, M.A., and Frydman, J. (2009). The chaperonin TRiC blocks a huntingtin sequence element that promotes the conformational switch to aggregation. Nat. Struct. Mol. Biol. *16*, 1279–1285.

Trettel, F., Rigamonti, D., Hilditch-Maguire, P., Wheeler, V.C., Sharp, A.H., Persichetti, F., Cattaneo, E., and MacDonald, M.E. (2000). Dominant phenotypes produced by the HD mutation in STHdh(Q111) striatal cells. Hum. Mol. Genet. *9*, 2799–2809.

Walsh, D.M., Thulin, E., Minogue, A.M., Gustavsson, N., Pang, E., Teplow, D.B., and Linse, S. (2009). A facile method for expression and purification of the Alzheimer's disease-associated amyloid beta-peptide. FEBS J. *276*, 1266–1281.

Wang, S., Sakai, H., and Wiedmann, M. (1995). NAC covers ribosome-associated nascent chains thereby forming a protective environment for regions of nascent chains just emerging from the peptidyl transferase center. J. Cell Biol. *130*, 519–528.

Wang, L., Zhang, W., Wang, L., Zhang, X.C., Li, X., and Rao, Z. (2010). Crystal structures of NAC domains of human nascent polypeptide-associated complex (NAC) and its αNAC subunit. Protein Cell *1*, 406–416.

Wang, F., Durfee, L.A., and Huibregtse, J.M. (2013). A cotranslational ubiquitination pathway for quality control of misfolded proteins. Mol. Cell *50*, 368–378.

Wegrzyn, R.D., Hofmann, D., Merz, F., Nikolay, R., Rauch, T., Graf, C., and Deuerling, E. (2006). A conserved motif is prerequisite for the interaction of NAC with ribosomal protein L23 and nascent chains. J. Biol. Chem. *281*, 2847–2857.

Wiedmann, B., Sakai, H., Davis, T.A., and Wiedmann, M. (1994). A protein complex required for signal-sequence-specific sorting and translocation. Nature *370*, 434–440.

STAR★METHODS

KEY RESOURCES TABLE

REAGENT or RESOURCE	SOURCE	IDENTIFIER
Antibodies		
GFP	Covance	RRID:AB_10063778
FLAG	Sigma-Aldrich	RRID:AB_262044
Actin	Santa Cruz	RRID:AB_2714189
Beta-NAC (BTF3)	Abcam	RRID:AB_1141066
HRP-anti-mouse IgG	Jackson	RRID:AB_2340771
HRP-anti-rabbit IgG	Jackson	RRID:AB_ 2340585
Alpha-NAC/Beta-NAC (C. elegans)	Kirstein-Miles et al., 2013	N/A
uL24 (C. elegans)	Deuerling lab	N/A
uL16 (RPL10L)	Abgent	Cat#AP17603a
Goat Anti-S tag	Abcam	RRID:AB_777789
Anti-6x HIS tag	Abcam	RRID:AB_2732046
RPLP0	Immunovision	Cat#HPO-0100
Tubulin	Gift from Thomas Mayer, University of Konstanz	N/A
Amyloid-beta (clone 6E10)	Absolute Antibody	Cat#ABA-AB00714-1.7
Bacterial and Virus Strains		
DH5α	Thermo-Fisher	Cat#18265017
OP50	CGC	Strain OP50
BL21 (DE3) Rosetta	Merck	Cat#70954
Rosetta 2 (DE3) pLysS	EMD Millipore	Cat#71401-4
Chemicals, Peptides, and Recombinant Proteins		
Complete EDTA-free protease inhibitor cocktail	Roche	Cat#5056489001
Cycloheximide	Sigma-Aldrich	Cat#C7698
DNase I	Sigma-Aldrich	Cat#DN25
Ni-IDA matrix, Protino	Roth	Cat#CN08.3
Floxuridine	LKT Laboratories	Cat#50-91-9
Levamisole	LKT Laboratories	Cat#16595-80-5
T4 DNA Ligase	New England Biolabs	Cat#M0202S
Phusion DNA Polymerase	Deuerling lab	N/A
C. elegans betaNAC N-term peptide	Genscript	Custom order, C-terminal amidation
Human betaNAC N-term peptide	Genscript	Custom order, C-terminal amidation
Human betaNAC N-term peptide (N-half)	Genscript	Custom order, C-terminal amidation
Human betaNAC N-term peptide (C-half)	Genscript	Custom order, C-terminal amidation
Human alphaNAC N-term peptide	Genscript	Custom order, C-terminal amidation
Sulfo-NHS Acetate	Thermo-Fisher	Cat#26777
GST-mHttQ51 recombinant protein	This paper	N/A
GST-Q51 recombinant protein	This paper	N/A
Ataxin-3 recombinant protein	This paper	N/A
NAC recombinant variants (C. elegans + human)	This paper	N/A
Ovalbumin	Sigma-Aldrich	Cat#A5503
acTEV protease	Thermo-Fisher	Cat#12575015
TNBS	G Biosciences	Cat#BC86
Glutathione Sepharose 4B	GE Healthcare	Cat#17-0756-05

(*Continued on next page*)

Continued

REAGENT or RESOURCE	SOURCE	IDENTIFIER
Cellulose acetate membrane OE66	GE Healthcare	Cat#10404180
7K MWCO Zeba Spin desalting columns	Thermo Fisher	Cat#89882
Strataclear Resin	Agilent	Cat#400714
BS3-d0/BS3-d4 (used for Ataxin-3-NAC xlinking)	Thermo-Fisher	Cat#10066323
Q Sepharose Fast Flow	GE Healthcare	Cat#17051001
GeneRuler 1 kb	Thermo-Fisher	Cat#SM0312
BS3-H12/BS3-d12 (used for Abeta40-NAC xlinking)	Creative Molecules	Cat#001SS
Ulp-1	Deuerling lab	N/A
Hsp-1 (Hsp-70)	This paper	N/A
Dnj-13 (Hsp40)	This paper	N/A
Firefly Luciferase	This paper	N/A
Protein G Agarose	Thermo-Fisher	Cat#20398
Critical Commercial Assays		
Proteostat Aggresome Detection Kit	Enzo Life Sciences	Cat#ENZ-51035-K100
CellTiter-Glo Luminescent Cell Viability Assay	Promega	Cat#G7572
Experimental Models: Cell Lines		
ST HDH Q7/7	Coriell Cell Repositories	Cat#CH00096
ST HDH Q7/111	Coriell Cell Repositories	Cat#CH00097
HEK293T	ATCC	Cat# CRL-3216
Experimental Models: Organisms/Strains		
N2	CGC	WormBase ID: N2
AM140 *rmIs132 [unc-54p::Q35::YFP]*	CGC	AM140
FlucDM-EGFP *marls135 [unc-54p::FlucDM::EGFP]*	Ulrich Hartl, Gupta et al., 2011	N/A
Oligonucleotides		
alphaNAC siRNA	Dharmacon	Cat#L-041821-01-0005
betaNAC siRNA	Dharmacon	Cat#L-052370-01-0005
Scrambled siRNA	Dharmacon	Cat#D-001206-14-05
Recombinant DNA		
pET11a-ataxin3-78Q	Generated in Radford lab. Orginal construct from Sandra Macedo-Ribeiro (Instituto de Biologia Molecular e Celular and Instituto de Investigação e Inovação em Saúde, University of Porto)	N/A
pETSac-mAβ40	Provided by Dr. Sara Linse (Lund University, Sweden) and Prof. Dominic Walsh (Harvard Institute of Medicine, USA).	N/A
pCFJ90 (myo-2p::mCherry)	Addgene, Frøkjaer-Jensen et al., 2008	RRID:Addgene_19327
pPD61_125	Addgene, gift from Andrew Fire	RRID:Addgene_1508
pPD61_125_myo-3p::3xFLAG-alphaNAC::unc-53-3′utr	This paper	N/A
pPD61_125_myo-3p::3xFLAG-betaNAC::unc-53-3′utr	This paper	N/A
pPD61_125_myo-3p::3xFLAG-deltaUBA-alphaNAC::unc-53-3′utr	This paper	N/A
pPD61_125_myo-3p::3xFLAG-RRK/AAA-betaNAC::unc-53-3′utr	This paper	N/A
pPD61_125_myo-3p::3xFLAG-deltaN-betaNAC::unc-53-3′utr	This paper	N/A
p6xHis-SUMO-Hsp-1 (Hsp70 expression vector)	This paper	N/A
p6xHis-SUMO-Dnj-13 (Hsp40 expression vector)	This paper	N/A

(*Continued on next page*)

Continued

REAGENT or RESOURCE	SOURCE	IDENTIFIER
pDS56-6xHis-Luciferase	This paper	N/A
p6xHis-SUMO-alphaNAC/betaNAC (C. elegans)	Kirstein-Miles et al., 2013	N/A
p6xHis-SUMO-alphaNAC/betaNAC (human)	This paper	N/A
p6xHis-SUMO-alphaNAC/RRK/AAA-betaNAC (C. elegans)	This paper	N/A
p6xHis-SUMO-alphaNAC/deltaN-betaNAC (C. elegans)	This paper	N/A
p6xHis-SUMO-deltaUBA-alphaNAC/betaNAC (C. elegans)	This paper	N/A
p6xHis-SUMO-deltaN-alphaNAC/deltaN-betaNAC (human)	This paper	N/A
Software and Algorithms		
Fiji Image software	Schindelin et al., 2012	https://fiji.sc/
Prism 7	Graphpad	https://www.graphpad.com/scientific-software/prism/
MassLynx 4.1	Waters	http://www.waters.com/waters/en_US/MassLynx-MS-Software
Peaks 7/8	Bioinformatics Solutions	http://www.bioinfor.com/peaks-studio/
StavroX	Götze et al., 2012	https://www.stavrox.com
Image Studio Lite	Li-Cor	https://www.licor.com/
ImageJ	NIH	https://imagej.nih.gov/ij/
WinDaq	DataQ Instruments	https://www.dataq.com

CONTACT FOR REAGENT AND RESOURCE SHARING

Further information and requests for reagents should be directed to Lead Contact Elke Deuerling (elke.deuerling@uni-konstanz.de).

EXPERIMENTAL MODEL AND SUBJECT DETAILS

Cell lines

Cell lines (ST HDH Q7/7 and ST HDH Q7/111) were purchased from the Coriell Cell Repository and not authenticated for this study. Cells were cultured in DMEM under 5% CO_2.

C. elegans strains

*C. elegan*s strain AM140 (*rmIs132 [unc-54p::Q35::YFP]*) was obtained from Caenorhabditis Genetics Center (CGC). Strain FlucDM-EGFP (*marIs135 [unc-54p::FlucDM::EGFP*] (Gupta et al., 2011) was obtained from Ulrich Hartl, Max-Planck-Institute of Biochemistry, Martinried, Germany. Worms were cultured according to standard techniques with *E. coli* OP50 as food source (Brenner, 1974).

METHOD DETAILS

Protein purification

PolyQ51 and mHttQ51 (Exon 1 of *HTT* with 51 glutamine repeat) plasmids were constructed as previously described (Tam et al., 2006). Proteins were expressed in Rosetta 2(DE3) pLysS competent cells (Agilent Technologies) in LB media supplemented with carbenicilin and chloramphenicol. Cultures were induced with 1 mM IPTG for 2.5h at 16°C. For purification, pellets were resuspended in 50 mM sodium phosphate, pH 8.0; 150 mM NaCl; 1 mM EDTA and lysed using an Emulsiflex (Avestin). Lysate was incubated with GSH-Sepharose resin (GE Healthcare) and washed with 0.1% (v/v) Triton, 500 mM NaCl, and 5 mM Mg-ATP before eluting protein with 15 mM glutathione. Protein was concentrated and buffer exchanged with 50 mM Tris-HCl, pH 8.0; 100 mM NaCl; 5% (v/v) glycerol. Concentrated protein was 0.2 μm filtered before storage at −80°C.

Wild-type NAC and NAC mutants from both human (αNAC = *NACA*; βNAC = *BTF3*) and *C. elegans* (αNAC = *icd-2*; βNAC = *icd-1*) were recombinantly expressed in Rosetta (DE3) cells as His-SUMO fusion constructs. Cultures were induced with 0.5 mM IPTG over night at 20°C. Cell pellets were resuspended in lysis buffer (20 mM sodium phosphate pH 7.5, 300 mM NaCl, 6 mM $MgCl_2$, 2 mM

β-mercaptoethanol, 2 mM PMSF, 10 μg/mL DNase I, 10% (v/v) glycerol) and lysed by French Press. Proteins were captured using Ni-IDA matrix (Protino; Macherey-Nagel) and eluted with lysis buffer containing 250 mM imidazole. Elution fractions were dialyzed overnight in the presence of 8 μg Ulp-1 per mg protein for proteolytic cleavage of the His-SUMO tag. Ion exchange chromatography using Resource Q column (GE Healthcare) was used for further purification. Elution fractions containing αNAC and βNAC in a 1:1 ratio were pooled, frozen in liquid nitrogen and stored at −80°C.

His-tagged AtxQ78 (*ATXN3*) was purified as described in Scarff et al. (Scarff et al., 2015) using nickel affinity chromatography and size-exclusion chromatography.

Aβ40 peptide was expressed and purified as described previously (Stewart et al., 2017; Walsh et al., 2009). In short, BL21 (DE3) cells were transformed with pETSac-mAβ40. Expression of Aβ40 was induced by the addition of IPTG to a final concentration of 1 mM. The cells were allowed to grow for an additional three hours before collection. Inclusion bodies were extracted from the cells by means of sonication followed by centrifugation. Aβ40 was purified from the inclusion body lysate by Q-Sepharose purification followed by two rounds of SEC. The purified peptides were lyophilized and stored at −20°C. The purity of the peptides was confirmed by SDS-PAGE and LC-MS.

In vitro aggregation assays

Mutant Huntingtin and PolyQ51 aggregation reactions were performed at concentration 3 μM of mHttQ51, 0.044 Units/μl acTEV protease (Invitrogen, Carlsbad, CA, USA), and respective concentrations of Ovalbumin (Sigma) or purified NAC chaperone variants. Aggregation was conducted in TEV reaction buffer (Invitrogen) and incubated at 30°C. AtxQ78 was buffer exchanged into TEV reaction buffer using 7K MWCO Zeba Spin Desalting Columns (Thermo Fisher) to initiate aggregation. AtxQ78 aggregation reactions were performed at 30 μM of Ataxin-3 in reaction buffer (20 mM sodium phosphate pH 7.5, 25 mM NaCl, 6 mM $MgCl_2$, 2 mM DTT, 5% (v/v) glycerol) and incubated at 37°C. Samples at varied time-points were then taken and combined in a 1:1 ratio with a 4% (w/v) SDS, 100 mM DTT solution, boiled for 5 min at 95°C, and stored at −20°C. Samples were then filtered through a 0.22 μm cellulose acetate membrane (Whatman) and washed with 0.1% (w/v) SDS. Membrane was probed using an S-tag antibody (Abcam) for mHttQ51 and PolyQ51, and with a His-tag antibody (Abcam) for AtxQ78.

Thioflavin T fluorescence assay

Lyophilized Aβ40 was resuspended at 320 μM in 20 mM sodium phosphate pH 7.4, 0.2 mM EDTA, 0.01% (w/v) sodium azide and stored on ice. The NAC proteins were diluted to 100 μM in storage buffer (20 mM sodium phosphate pH 7.5, 25 mM NaCl, 6 mM $MgCl_2$, 2 mM β-mercaptoethanol, 5% (v/v) glycerol) and buffer exchanged into 20 mM sodium phosphate pH 7.4, 0.2 mM EDTA, 0.01% (w/v) sodium azide, 1x complete^{TM} mini protease inhibitor, EDTA free (Roche) by means of ZebaSpin 7 kDa MWCO spin columns (Thermo Scientific). Samples were prepared that contained equimolar concentrations of Aβ40 and NAC variants. Thioflavin T was added to a final concentration of 10 μM. The samples were transferred to a 96 well half-area clear bottom microplate (Corning GmbH, Wiesbaden, Germany), with 95 μL of sample in each well. The fluorescence (excitation: 440 nm, emission: 480 nm) was measured using a BMG Omega plate reader (BMG Labtech) incubating samples at 37°C, quiescently.

Transmission electron microscopy

After 20 h, samples were taken from the Thioflavin T plate and fixed on carbon coated copper grids, made in house. The samples were negative stained with 2% (w/v) uranyl acetate. The samples were imaged on a JEOL 1400 TEM at the Astbury structural biology laboratory, University of Leeds.

Cell viability assays and real-time PCR

siRNA knockdown was completed using the DharmaFECT reverse transfection protocol. Striatal knock-in cell lines (homozygous wild-type HttQ7/7 and heterozygous mutant HttQ7/111) were plated in 96-well plates (1.25 × 10^4 cells/well) in complete medium (DMEM with high glucose, 10% FBS) at 32°C. Experiments were plated to have four technical replicates per siRNA treatment for each experiment, with each independent experiment repeated at least three times. 72 hours post transfection, cells were incubated with Cell Titer Glo reagent (Promega) for at least 10 min before recording luminescence signal. For real-time PCR (RT-PCR), RNA was harvested from cells using the Zymo Quick-RNA kit, cDNA was synthesized using the iScript kit. RT-PCR was completed using the SYBR Green Master Mix from Biorad and fold-knockdown was calculated using the $2^{-\Delta\Delta Ct}$ method.

Fluorescence microscopy of cells

Cells were imaged on a Zeiss LSM 700 confocal microscope (Carl Zeiss). Cells were prepared similarly as above but plated on a poly-lysine coated coverslip in 24-well plate. Post transfection, the cells were stained with a 1:2000 Proteostat solution (Enzo Life Sciences, Farmingdale, NY, USA) for 1 hour, followed by a 0.67 μg/mL Hoechst stain for 5 min, prior to imaging. For proteasome inhibition, cells were treated with 5 μM MG132 for 6 hours prior to imaging.

Polysome analysis in human cells

Prior to harvesting, HEK293T cells were treated with 100 μg/mL cycloheximide (CHX) for 5 min at 37C. Cells were then washed twice in 100 μg/mL CHX in PBS and harvested in the same buffer on ice. Pelleted cells were then resuspended in lysis buffer (10 mM

HEPES pH 7.9, 1.5 mM $MgCl_2$, 10 mM KCl, 0.5 mM DTT, 1% Triton X-100, 100 μg/mL CHX) and lysed by trituration through a 26G needle for 10 passes. The sample was centrifuged at 1500 x g for 5 min at 4°C. RNA concentration of the supernatant was then measured by Nanodrop. 200 μg (in RNA) of lysate was loaded onto a 12 mL 10%–50% (w/v) linear sucrose gradient (Gradient Mate, Biocomp Instruments) prepared in gradient buffer (100 mM KCl, 20 mM HEPES pH 7.6, 5 mM $MgCl_2$, 100 μg/mL CHX, 1U/μl RNase inhibitor) and centrifuged for 2 h at 36000 rpm in a swinging bucket rotor (SW-41, Beckmann). Gradients were then fractionated from top to bottom with a density gradient fractionator (Brandel), and A260 was monitored to detect cytosolic fractions, ribosomal subunits, monosomes, and polysomes. Data were recorded and processed with WinDaq (Dataq Instruments). For one gradient, 15 fractions with 1 mL each were collected. For subsequent western analysis, 500 μl of gradient buffer and 10 μl of Strataclear resin slurry (Agilent Technologies) was added to each fraction and incubated on rotation at 4°C. Fractions were centrifuged twice at 3000 x g at 4°C for 5 min to remove supernatant. The remaining resin was then resuspended in 20 μl 2X Laemmli Buffer, centrifuged at 3000 x g for 5 min, and the residual supernatant was loaded into an SDS-PAGE gel and then transferred onto a nitrocellulose membrane. Different dilutions of primary antibodies were applied (1:400 anti-βNAC, 1:3000 anti-RPLP0).

Sulfo-NHS peptide labeling

NAC N-terminal peptides were ordered from Genscript. Peptides were dissolved to 1 mM in 0.1 M sodium carbonate buffer, pH 8.5. Peptide solutions were added to a 25-fold molar excess of Sulfo-NHS Acetate (Thermo Scientific, Waltham, MA, USA) to amine groups in the sample and incubated for 1 hour at room temperature. Reaction was quenched using a 1 M Tris-HCl, pH 7.5 solution. To quantify the efficiency of this labeling, a lysine standard curve was established; samples were assayed for free primary amines by adding 0.01% (w/v) TNBS in 0.1 M sodium bicarbonate, pH 8.5 solution (G Biosciences) to each sample and standard, and incubated at 37°C for 2 hours. 10% SDS and 1N HCl was then added to stop the reaction. Absorbance was measured at 335 nm.

Chemical crosslinking and mass spectrometry

For crosslinking AtxQ78 was buffer exchanged into 10 mM sodium phosphate (pH 7.2) and added to NAC at a 1:1 ratio (20 μM NAC + 20 μM AtxQ78). A 1:1 mixture of BS^3-d^0 and BS^3-d^4 was added to the proteins at 20x and 50x molar excess and the reaction allowed to proceed at room temperature for 1 hour before quenching with the addition of 50 mM Tris-Cl (pH 7.5). Samples were diluted with 2x loading buffer and separated on Tris-tricine gels followed by staining with InstantBlue (Expedeon).

Aβ40 (18 μM) was incubated with purified NAC in a 1:1 molar ratio in Aβ aggregation buffer (20 mM sodium phosphate pH 7.5, 0.2 mM EDTA, 0.01% (w/v) NaN_3) at 37°C for 2 h. BS^3-$h^{12}d^{12}$ was added to the proteins at 20x molar excess and incubated for 30 min at 37°C before quenching with 50 mM NH_4HCO_3. Crosslinked samples were gel-filtrated using a Superdex 75 column (GE Healthcare) and fractions containing crosslinked Aβ40-NAC complexes subjected to co-immunoprecipitation using Aβ antibody 6E10 (Biozol). Captured proteins were denatured with 1x SDS sample buffer under non-reducing conditions to avoid splitting of the antibody in heavy and light chains.

Gel pieces containing the crosslinked complexes were washed with 25 mM ammonium bicarbonate (pH 7.8) for 1 h with shaking. The solution was removed and the pieces destained three times with 25 mM ammonium bicarbonate in 60% acetonitrile. Gel pieces were dehydrated with 100% acetonitrile for 10 min and left to air-dry in a laminar flowhood for 1 h. Rehydration of the gel pieces was achieved by adding 0.1 mg/mL trypsin solution and incubating the samples on ice for 30 min. Excess trypsin was removed and the samples were incubated at 37°C and 1000 rpm overnight. Peptides were extracted from the gel using 3 washes with 60% acetonitrile/ 5% formic acid. The extracts were pooled and concentrated using a SpeedVac before being analyzed using a nanoACQUITY LC-system coupled to a Synapt HDMS G2Si mass spectrometer. Peptides were injected onto a C18 column equilibrated with 0.1% formic acid in water and eluted using an increasing gradient of 0.1% formic acid in acetonitrile over 60 min at a flow rate of 0.3 μl/min. The Synapt HDMS G2Si was operated in positive mode using a capillary voltage of 3.0 kV, cone voltage of 40 V, backing pressure of 3.6 mbar and a trap bias of 2.0 V. The source temperature was 80°C and the trap pressure was 8.70×10^{-3} mBar. Glu-fibrinogen and Leucine Enkephalin were infused as lock mass calibrants. Data acquisition was achieved using Data Dependent Analysis (DDA) with a one second MS scan over an *m/z* range of 250–3000 being followed by three 1 s MS/MS scans taken from the five most intense ions in the MS spectrum over an *m/z* range of 50–2000. Data processing was performed using the MassLynx v4.1 suite of software supplied with the mass spectrometer and PEAKS 7/8 (Bioinformatics Solutions). Crosslinks were identified using StavroX software (Götze et al., 2012) and verified manually.

Luciferase refolding assay

Firefly Luciferase refolding activity was measured as previously described (Sun et al., 2012). Recombinant luciferase (2.5 μM) was chemically denatured for 45 min at room temperature in denaturing buffer (25 mM HEPES/KOH, pH 7.4, 50 mM KCl, 15 mM MgCl2, 1 mM ATP, 10 mM DTT, 0.05 mg/mL BSA, 5 M GdmCl). To test for refolding activity, 0.02 μM denatured luciferase was preincubated in the presence or absence of 0.02 μM NAC variants for 15 min at room temperature. Luciferase refolding was induced by addition of 3.2 μM CeHsc70 (HSP-1), 0.8 μM CeHsp40 (DNJ-13) and luminescence buffer (75 mM HEPES/KOH, pH 7.4, 50 mM KCl, 15 mM $MgCl_2$, 1 mM ATP, 2 mM DTT, 0.05 mg/mL BSA, 240 μM Coenzyme A, 0.1 mM luciferin, 10 mM PEP, 50 μg/mL pyruvate kinase). Luminescence was measured in 96-well LIA-plates (Greiner) over 2 hours at room temperature in a microplate reader (BertholdTech TriStar2S).

C. elegans transformation

Transgenic strains were generated using standard microinjection protocols (Mello and Fire, 1995). Constructs for overexpression of NAC in body wall muscles were generated by cloning the coding sequences of *icd-1* (βNAC) and *icd-2* (αNAC) into pPD61_125 vector containing the *myo-3* promoter and the *unc-54* 3′ untranslated region (UTR). The NAC genes were N-terminally tagged with 3x FLAG. Mutant NAC constructs were generated by standard mutagenesis protocols. AM140 (*rmIs132 [unc-54p::Q35::YFP]*) and FlucDM-EGFP (*marIs135 [unc-54p::FlucDM::EGFP]*) worms were injected with 25 ng/μl of each NAC plasmid together with CFJ90 *myo-2*p::mCherry (2.5 ng/μl) (Frøkjaer-Jensen et al., 2008) and DNA ladder (100 ng/μl, GeneRuler 1 kb, Thermo Scientific). Control strains were obtained by injecting 50 ng/μl empty vector, 2.5 ng/μl *myo-2*p::mCherry and 100 ng/μl DNA ladder. For each transformation, at least two independent transgenic lines carrying extrachromosomal arrays were obtained showing similar results. Detailed strain information is available in Table S3.

Synchronization of *C. elegans*

Synchronization of worms for microscopic studies was carried out by a timed egg-lay for 5 h. Large age-synchronized *C. elegans* cultures for SDD-AGE analyses were obtained by collecting embryos from gravid adult worms using a 20% alkaline hypochlorite bleaching for 5 min. Embryos were allowed to hatch overnight in M9 buffer to get arrested L1s. Transgenic L1 larvae were sorted based on the *myo-2*p::mCherry marker using a COPAS FlowPilot system (Union Biometrica). The synchronized, transgenic L1s were transferred to OP50 seeded plates and incubated at 20°C. After two days the young adult worms were transferred to new plates containing 150 μM 5-fluorodeoxyuridine (LKT Laboratories) to prevent the culture from reproducing.

Fluorescence microscopy of worms

Worms were immobilized on 3% agarose pads and anaesthetized using 25 mM levamisole (LKT Laboratories). Images were taken with a confocal laser-scanning microscope TCS SP8 (Leica) with 5x (whole body images) and 63x objectives (head region). Images were adjusted as necessary in Fiji (ImageJ) (Schindelin et al., 2012) using cropping, brightness and contrast tools.

SDD-AGE

SDD-AGE was carried out as previously described (Halfmann and Lindquist, 2008). For sample preparation, worms were extracted in lysis buffer (100 mM Tris-Cl pH 7.5, 50 mM NaCl, 10 mM β-mercaptoethenol, 1x complete protease inhibitor) by sonication (four times, 10 pulses, duty cycle = 40, output control = 2; Branson sonifier). Lysed worms were centrifuged for 1 min at 500 g to remove debris and the supernatant was transferred to a new tube. ¼ volume of 4x SDD-AGE sample buffer (2x TAE, 20% glycerol, 8% SDS, 0.05% bromphenol blue) was added to the lysates and incubated for 15 min at RT. Samples were loaded onto a 1.2% agarose gel in 1x TAE buffer (40 mM Tris-Cl, pH 7.6, 20 mM acetic acid, 1 mM EDTA) containing 0.1% SDS and proteins were blotted on nitrocellulose membranes by capillary transfer in 1x Tris buffer (150 mM NaCl, 50 mM Tris-Cl pH 7.5) over night at room temperature. The membrane was analyzed using an anti-GFP antibody (Covance).

Polysome analysis of worms

C. elegans N2 worms were cultivated in liquid culture at 20°C in presence of *E. coli* OP50 as food source. Day 2 post-L4 worms were harvested on ice with 0.1 M NaCl and seperated from bacteria via sucrose floatation. After an additional washing step the nematodes were flash frozen in liquid nitrogen. Worm pellets were cryo-genic grinded using a cryo-mill (Retsch) for 30 s at 22 Hz. Frozen worm powder was resuspended in lysis buffer (30 mM HEPES/KOH pH 7.4, 50 mM KoAc, 5 mM $MgCl_2$, 5% (w/v) mannitol, 100 μg/mL cycloheximide, 2 mM β-mercaptoethanol, 1 x complete protease inhibitor) and centrifuged at 18,000 g for 15 min at 4°C. The supernatant was adjusted to 20 A_{260} U/mL and 500 μl were loaded on a sucrose gradient (15%–45% in lysis buffer). Ribosomal species were separated by ultracentrifugation (TH-641 rotor) at 39,000 rpm for 2.5 hours (4°C). Gradients were fractionated using a density gradient fractionator (Teledyne Isco, Inc.) monitoring the A_{254} and fractions were directly analyzed by immunoblotting.

Paralysis assay

To analyze the percentage of paralyzed worms, 100 semi-synchronized (timed egg lay for 5 h) young adult worms of each strain were placed on a plate containing 150 μM 5-fluorodeoxyuridine. Screening of paralyzed worms was started at day 6 of adulthood. Worms were scored as paralyzed when they only moved their heads but failed to undergo a full body wave propagation upon repeated prodding with a platinum wire worm picker.

Immunoblot analysis in *C. elegans*

Protein samples were applied to SDS–PAGE and electroblotted onto nitrocellulose membranes according to standard protocols. Commercial antibodies used throughout this study were GFP (Covance, MMS-118P), FLAG (Sigma, F1804), Actin (Santa Cruz, sc-47778), and uL16 (Abgent, AP176039). Polyclonal antibody against *C. elegans* NAC (αNAC + βNAC) was described previously (Kirstein-Miles et al., 2013). Antibody against uL24 was raised in rabbits immunized with recombinant full-length *C. elegans* RPL-26 protein. Tubulin antibodies were a kind gift from Thomas Mayer, University of Konstanz. Blots were probed with secondary antibodies coupled to HRP (Jackson, anti-mouse 715-035-151; anti-rabbit 711-005-152).

QUANTIFICATION AND STATISTICAL ANALYSIS

Experimental procedure

Each experiment was conducted at least three times to generate three biological repeats. For western blots, dot blots, and fluorescence microscope images the most representative experiment is shown.

Statistics

Bar graphs for quantifications show the average of at least three independent experiments ± SEM. Statistical parameters, including the exact value of n and statistical significance are reported in the Figure Legends. Data are judged to be statistically significant when $p < 0.05$ by the comparison test indicated in the Figure legends. In figures, asterisks denote statistical significance (*, $p < 0.05$, **, $p < 0.01$, ***, $p < 0.001$) as compared to appropriate controls.

DATA AND SOFTWARE AVAILABILITY

Raw data have been deposited to Mendeley Data and are available at https://doi.org/10.17632/r6dgtfjt2y.1.

Molecular Cell, Volume *74*

Supplemental Information

Dual Role of Ribosome-Binding Domain of NAC as a Potent Suppressor of Protein Aggregation and Aging-Related Proteinopathies

Koning Shen, Martin Gamerdinger, Rebecca Chan, Karina Gense, Esther M. Martin, Nadine Sachs, Patrick D. Knight, Renate Schlömer, Antonio N. Calabrese, Katie L. Stewart, Lukas Leiendecker, Ankit Baghel, Sheena E. Radford, Judith Frydman, and Elke Deuerling

Figure S1

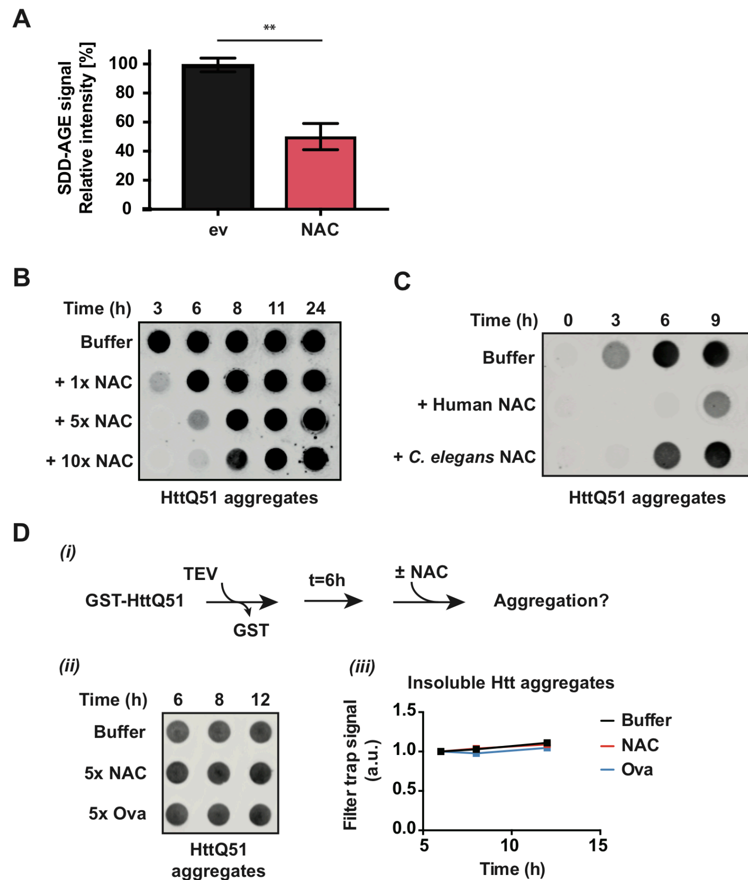

Figure S1. Aggregation suppression of mutant Huntingtin by NAC. Related to Figure 1.
(A) Quantification of PolyQ35::YFP signal on SDD-AGE blots as shown in Figure 1B. Data are represented as mean ± SEM (n = 3). Statistical significance was calculated by Student's t test. ev = empty vector.
(B) *In vitro* filter trap aggregation assay of mutant Huntingtin (mHttQ51) incubated with 1x, 5x or 10x molar excess of human NAC. Aggregation of GST-mHttQ51 was initiated by cleavage of the GST tag using the TEV protease. SDS-insoluble aggregates were detected with an S-tag antibody.
(C) Same assay as in (A) but with either human or *C. elegans* NAC added.
(D) (*i*) Schematic of *in vitro* filter trap aggregation assay of mHttQ51. Experiment was conducted similarly to (A), with the exception of a 6-hour time delay between initiation of aggregation and addition of NAC or Ovalbumin control. (*ii*) SDS-insoluble aggregates of mHttQ51 after addition of 5x molar excess of NAC or ovalbumin (Ova) control. (*iii*) Quantification of SDS-insoluble aggregates shown in (*ii*).

Figure S2

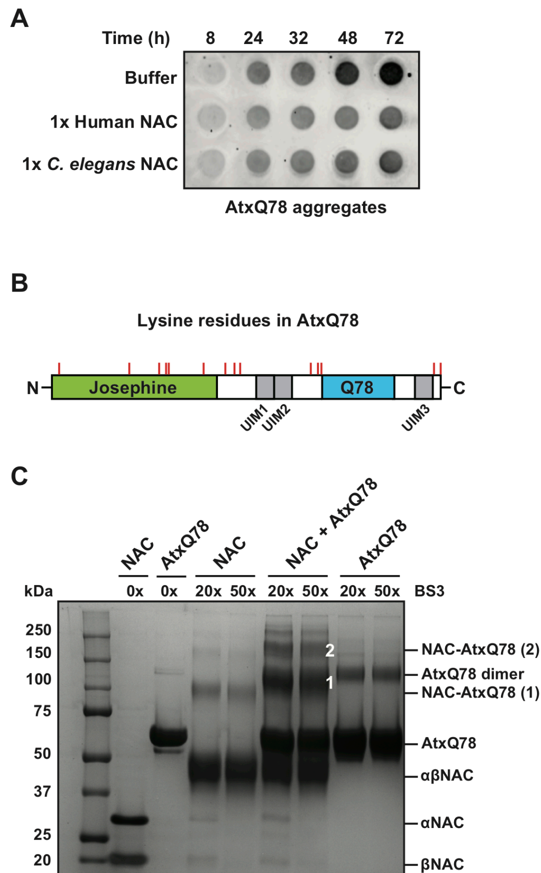

Figure S2. Interaction of NAC with mutant Ataxin-3. Related to Figure 2.

(A) Filter trap aggregation assay of AtxQ78 incubated with an equimolar concentration of either human or *C. elegans* NAC at 37°C for the indicated time. SDS-insoluble aggregates were detected with an anti-His antibody.

(B) Schematic showing the domain architecture of Ataxin-3. All lysine residues carrying optimal functional groups for chemical crosslinking with amine-reactive crosslinkers are highlighted in red. Josephine domain, green. PolyQ78 stretch, blue. UIM = ubiquitin interacting motif.

(C) Coomassie-stained Tris-Tricine gel showing crosslinked protein complexes. NAC and AtxQ78 were crosslinked either with 20x or 50x molar excess of BS3 for 1 hour. NAC and AtxQ78 alone were used as controls. New bands labeled with 1 (NAC-AtxQ78 monomer) and 2 (NAC-AtxQ78 dimer) were excised from the gel and subjected to an in-gel digest for the LC-MS analysis shown in Figure 2C.

Figure S3

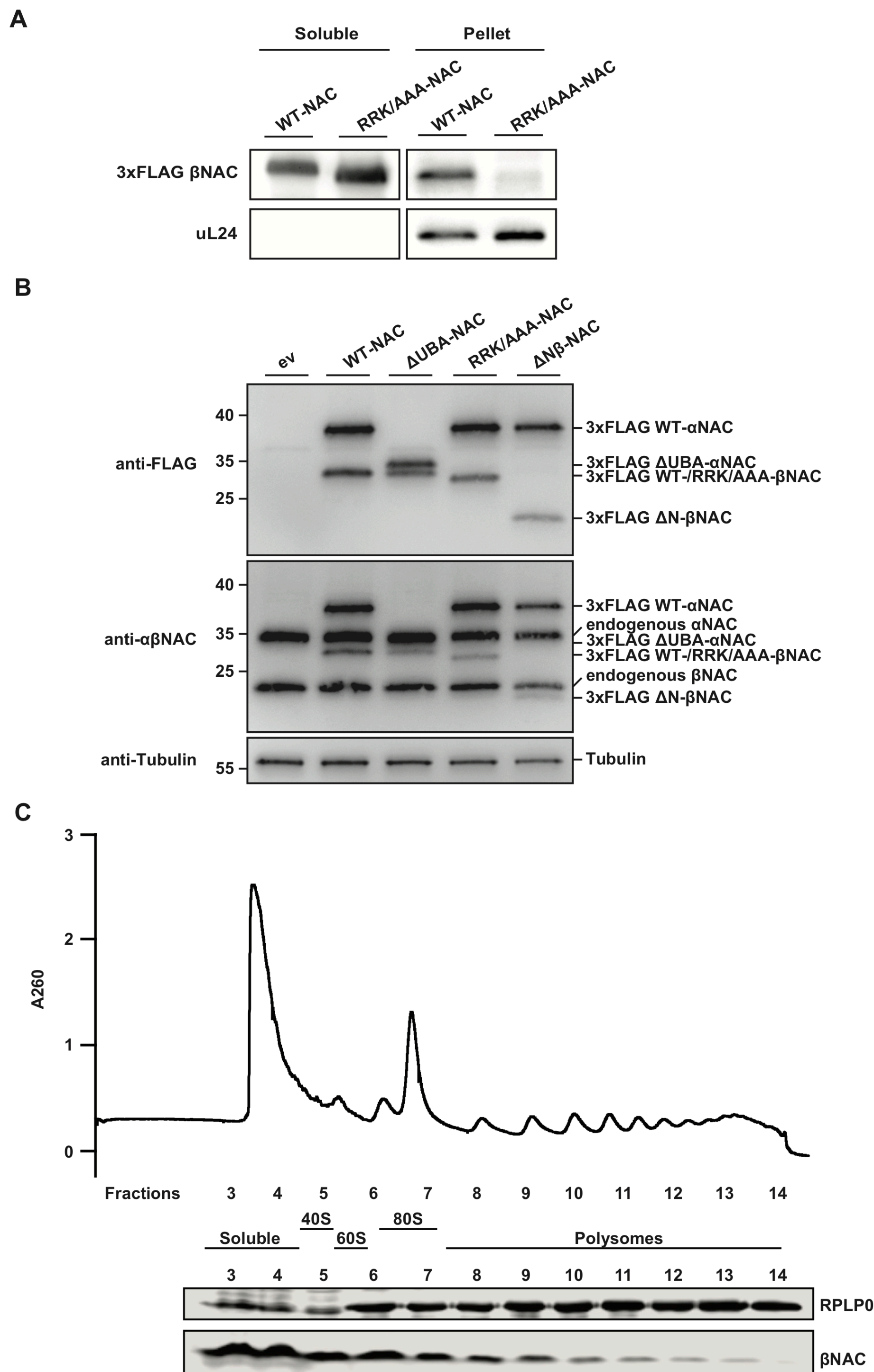

Figure S3. Association of NAC with ribosomes. Related to Figure 3.
(A) Sucrose cushion centrifugation of ribosomes in PolyQ35::YFP *C. elegans* worms overexpressing either 3xFLAG-tagged WT- or RRK/AAA-NAC in muscle cells (*myo-3* promoter). Analysis was performed on day 2 of adulthood. Indicated proteins in the supernatant (Soluble) and ribosomal pellet (Pellet) fractions were analyzed by immunoblotting. uL24 served as a ribosomal marker.
(B) Immunoblot analysis of total levels of endogenous NAC (ubiquitous expression) and overexpressed 3xFLAG-tagged NAC variants in body wall muscles in animals investigated in Figure 3C, D. FLAG immunoblot shows only exogenously overexpressed NAC in muscle cells, while the αβNAC immunoblot shows endogenous and exogenous NAC variants, as indicated. Tubulin served as a loading control.
(C) Polysome profile of HEK293T cells. βNAC levels were assessed by immunoblotting. RPLP0 served as a ribosomal marker.

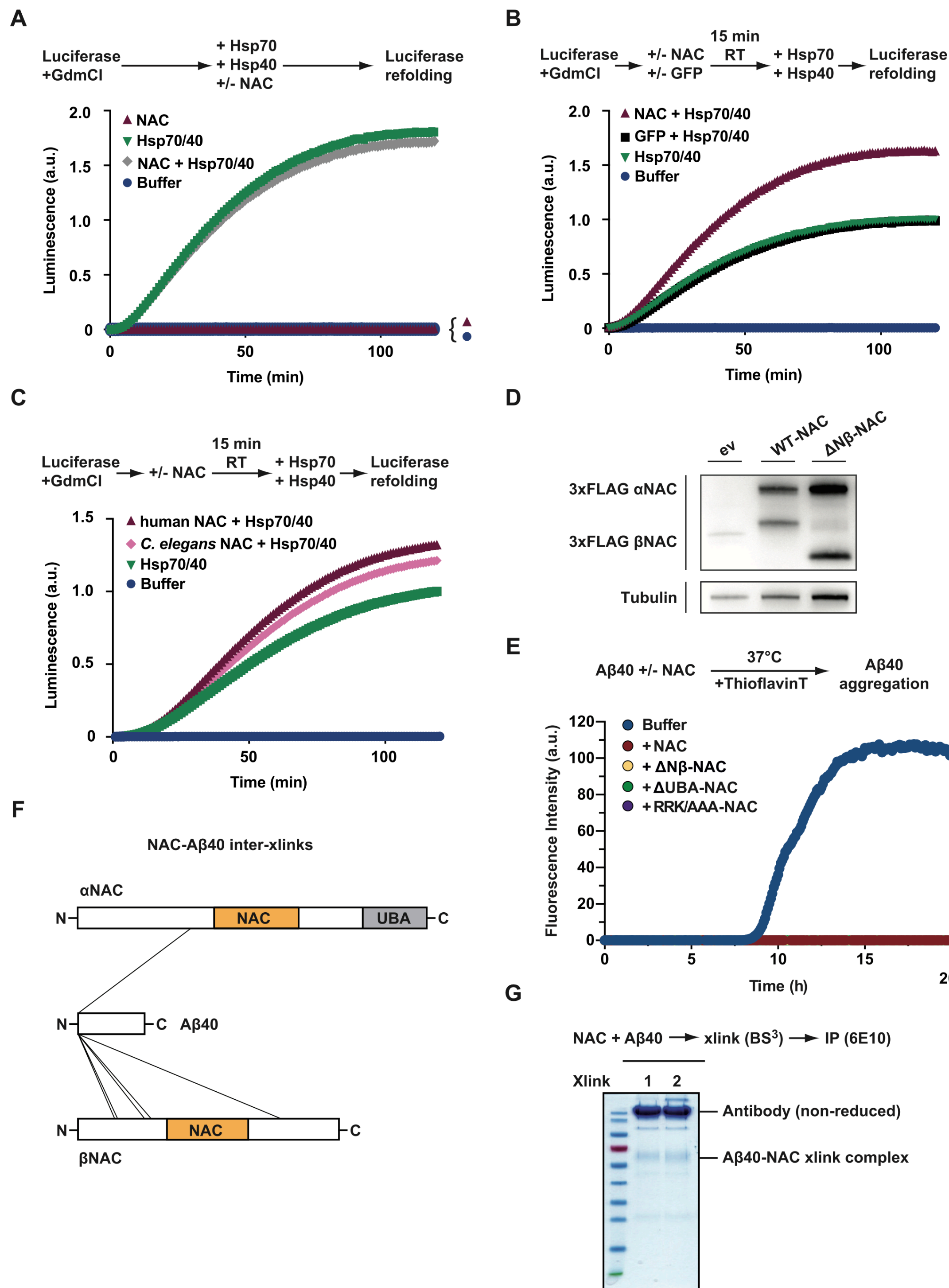

Figure S4. Chaperone activity of NAC on luciferase and Aβ40. Related to Figure 4.
(A) *In vitro* luciferase refolding assays using guanidine-HCl (GdmCl)-denatured substrate. Luciferase (0.02 μM) was incubated with an equimolar concentration of human NAC in the presence and absence of an Hsp70/Hsp40 system (3.2 μM/0.8 μM). Luciferase reactivation was analyzed by luminescence recording over two hours at RT using luciferin as a substrate. a.u. = arbitrary units.
(B) Similar assay as in (A) but luciferase was first preincubated with NAC or GFP control in a 1:1 molar ratio for 15 min at room temperature before adding the Hsp70/Hsp40 chaperone system.
(C) Experiment was conducted similarly to (B) but with NAC from both human and *C. elegans*.
(D) Immunoblot analysis of wild-type NAC and ΔNβ-NAC (FLAG-tagged α- and βNAC) overexpressed in FlucDM-EGFP strain. Tubulin served as loading control.

(E) Aβ40 aggregation (18 μM) was examined in the presence of molar equivalent *C. elegans* NAC constructs (18 μM) with 10 μM thioflavin T (ThT). Samples were incubated quiescently at 37°C for 20 h. Each color indicates replicate assays prepared in the same plate. Aggregation results were baseline subtracted from NAC constructs alone (without Aβ40) or buffer, which did not show aggregation.
(F) Crosslinked NAC-Aβ40 complexes from gel shown in (D) were excised and subjected to an in-gel digest and LC-MS analysis. Schematic shows identified intermolecular crosslinks. See also Table S2.
(G) Coomassie-stained gel showing isolated NAC-Aβ40 complexes crosslinked with BS^3. NAC and Aβ40 (both 18 μM) were incubated at 37°C for two hours and crosslinked using 20x molar excess of BS3 for 30 min. Crosslinked samples were gel-filtrated and NAC-Aβ40 complexes immunoprecipitated using Aβ40 antibody (6E10). Proteins were eluted under non-reducing conditions to avoid antibody splitting into light and heavy chains.

Figure S5

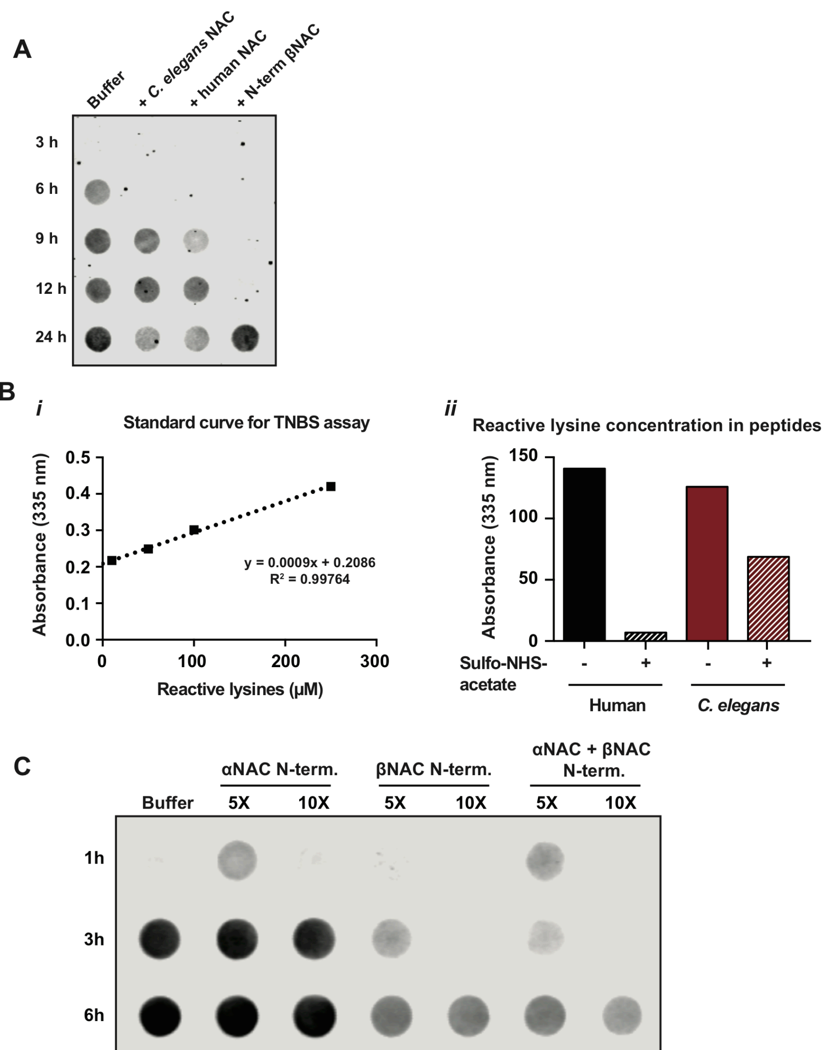

Figure S5. Suppression of PolyQ aggregation by βNAC N-terminus. Related to Figure 5.
(A) In vitro filter trap aggregation assay of PolyQ51 incubated with 5x molar excess of either *C. elegans* NAC, human NAC or the human N-terminal βNAC peptide. Aggregation of GST-PolyQ51 was initiated by cleavage of the GST tag using the TEV protease. SDS-insoluble aggregates were detected with an S-tag antibody.
(B) Quantification of sulfo-NHS-acetate labeling of lysine residues in βNAC N-terminal peptides using the TNBS assay to assess amount of primary amines. (*i*) Standard curve of lysine amino acid with 335 nm absorbance levels. (*ii*) Quantification of primary amine availability with differently treated peptides.
(C) *In vitro* filter trap aggregation assay of mutant Huntingtin (mHttQ51) incubated with 5x or 10x molar excess of human α- or βNAC N-terminal peptides as indicated. SDS-insoluble aggregates were detected with an S-tag antibody.

Figure S6

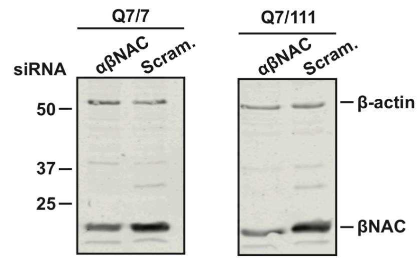

Figure S6. Knockdown efficiency of NAC in Q7/7 and Q7/111 cell lines. Related to Figure 6. Western blot showing βNAC knockdown in siRNA-treated cell lines used in viability assay shown in Figure 6A. β-actin was probed simultaneously as a loading control.

Table S1

Intra- and intermolecular NAC crosslinks. Related to Figure 2.

Score	m/z	z	M+H+	Calculated	Deviation	Peptide 1	Protein 1	From	To	Peptide 2	Protein 2	From	To	Site 1	Site 2
231	594.99	3	1782.956	1782.953	1.31	[QAK]	alpha-NAC	52	54	[VAEAAGLGDHIDK]	alpha-NAC	39	51	K3	K13
124	593.648	3	1778.929	1778.928	0.47	[VAEAAGLGDHIDKQAK]	alpha-NAC	39	54	0	dead-end	0	0	K13	x0
111	1140.91	3	3420.702	3420.686	4.87	[DDGTVIHFNNPK]	beta-NAC	70	81	[VQTSVPANTFSVTGSADNK]	beta-NAC	82	100	K12	T3
106	464.925	3	1392.76	1392.759	0.33	[KLQAQQEHVR]	beta-NAC	13	22	0	dead-end	0	0	K1	x0
95	550.95	3	1650.834	1650.837	-1.49	[QKEVK]	alpha-NAC	9	13	{MTGSTETR]	alpha-NAC	0	8	K2	{0
83	817.758	3	2451.258	2451.255	1.41	[IEDLTQHAQMSAIENLKPTR]	alpha-NAC	114	133	0	dead-end	0	0	K17	x0
75	711.375	3	2132.111	2132.109	0.61	[VAEAAGLGDHIDKQAKQSR]	alpha-NAC	39	57	1	intrapeptidal	0	0	K13	K16
73	539.313	3	1615.926	1615.928	-1.36	[IKKLQAQQEHVR]	beta-NAC	11	22	1	intrapeptidal	0	0	K2	K3
66	823.088	3	2467.251	2467.25	0.43	[IEDLTQHAQmSAIENLKPTR]	alpha-NAC	114	133	0	dead-end	0	0	K17	x0
66	640.038	3	1918.099	1918.105	-2.95	[SKNILFVINKPDVFK]	alpha-NAC	85	99	0	dead-end	0	0	K2	x0
61	593.647	3	1778.928	1778.928	-0.37	[VAEAAGLGDHIDKQAK]	alpha-NAC	39	54	0	dead-end	0	0	K16	x0
57	632.037	3	1894.097	1894.101	-1.82	[LGLK]	alpha-NAC	69	72	[LANNVTKLGPDGK]	beta-NAC	124	136	K4	K13
52	551.948	3	1653.829	1653.83	-0.35	[VCIRK]	alpha-NAC	80	84	{mTGSTETR]	alpha-NAC	0	8	K5	{0
52	1139.56	3	3416.655	3416.66	-1.62	[DDGTVIHFNNPK]	beta-NAC	70	81	[VQTSVPANTFSVTGSADNK]	beta-NAC	82	100	K12	T3
52	1139.56	3	3416.655	3416.66	-1.62	[DDGTVIHFNNPKVQTSVPANTFSVTGSADNK]	beta-NAC	70	100	0	dead-end	0	0	K12	x0
48	676.735	3	2028.19	2028.189	0.23	[KSKNILFVINKPDVFK]	alpha-NAC	84	99	1	intrapeptidal	0	0	K1	K3
45	602.312	3	1804.92	1804.922	-0.98	[IGGKGTPR]	beta-NAC	23	30	{MTGSTETR]	alpha-NAC	0	8	K4	{0
44	823.085	3	2467.241	2467.25	-3.39	[IEDLTQHAQmSAIENLKPTR]	alpha-NAC	114	133	0	dead-end	0	0	K17	x0
44	817.756	3	2451.254	2451.255	-0.36	[IEDLTQHAQMSAIENLKPTR]	alpha-NAC	114	133	0	dead-end	0	0	K17	x0
43	712.717	3	2136.136	2136.134	0.82	[LGPDGK]	beta-NAC	131	136	{mMDSKAIAERIK]	beta-NAC	0	12	K6	K12
42	817.758	3	2451.259	2451.255	1.59	[IEDLTQHAQMSAIENLKPTR]	alpha-NAC	114	133	0	dead-end	0	0	K17	x0
37	906.168	3	2716.488	2716.495	-2.73	[QITEMLPGILNQLGPESLTHLKK]	beta-NAC	101	123	0	dead-end	0	0	K23	x0
36	911.505	3	2732.502	2732.49	4.16	[QITEmLPGILNQLGPESLTHLKK]	beta-NAC	101	123	0	dead-end	0	0	K22	x0
35	433.451	5	2163.225	2163.229	-2.11	[IGGKGTPR]	beta-NAC	23	30	[KLQAQQEHVR]	beta-NAC	13	22	K4	K1
35	747.379	3	2240.121	2240.131	-4.09	[QVTGVSR]	alpha-NAC	73	79	[DDGTVIHFNNPK]	beta-NAC	70	81	S6	K12
34	607.644	3	1820.917	1820.917	-0.13	[IGGKGTPR]	beta-NAC	23	30	{mTGSTETR]	alpha-NAC	0	8	K4	T2
31	751.723	3	2253.153	2253.162	-3.61	{mTGSTETR]	alpha-NAC	0	8	[QSRSEKKARK]	alpha-NAC	55	64	{0	K6
29	816.777	3	2448.317	2448.313	1.8	[AIAERIK]	beta-NAC	6	12	{mTGSTETRQKEVK]	alpha-NAC	0	13	K7	T2
28	711.375	3	2132.111	2132.109	0.83	[LGPDGK]	beta-NAC	131	136	{mMDSKAIAERIK]	beta-NAC	0	12	K6	K12
26	556.282	3	1666.831	1666.832	-0.36	{mTGSTETRQKEVK]	alpha-NAC	0	13	0	dead-end	0	0	T5	x0
26	772.085	3	2314.24	2314.236	1.82	[QAKQSR]	alpha-NAC	52	57	[DIELVISQANTTR]	alpha-NAC	160	172	K3	T12
25	772.085	3	2314.241	2314.236	2.25	[QAKQSR]	alpha-NAC	52	57	[DIELVISQANTTR]	alpha-NAC	160	172	K3	T12
24	978.107	3	2932.308	2932.319	-3.91	{mTGSTETR]	alpha-NAC	0	8	[GEDEDVPELVGDFDAASK]	beta-NAC	137	154	S4	K18
24	691.408	3	2072.21	2072.201	4.58	[IGGK]	beta-NAC	23	26	[QVTGVSRVCIRKSK]	alpha-NAC	73	86	K4	S6
23	691.408	3	2072.21	2072.212	-0.84	[KAR]	alpha-NAC	61	63	[QVTGVSRVCIRKSK]	alpha-NAC	73	86	K1	S6
22	556.282	3	1666.831	1666.832	-0.36	[EVK]	alpha-NAC	11	13	{mTGSTETRQK]	alpha-NAC	0	10	K3	T5
21	1032.54	3	3095.601	3095.612	-3.42	[SEKKARKLFSK]	alpha-NAC	58	68	[EADNDIVNAIMSLTM}	alpha-NAC	181	196	K11	T14
20	478.29	3	1432.854	1432.852	1.2	[QSR]	alpha-NAC	55	57	[LFSKLGLK]	alpha-NAC	65	72	S2	K8
18	550.277	3	1648.815	1648.821	-3.71	{mTGSTETRQKEVK]	alpha-NAC	0	13	1	intrapeptidal	0	0	{0	K10
18	736.346	3	2207.025	2207.029	-1.93	{MTGSTETR]	alpha-NAC	0	8	{mmDSKAIAER]	beta-NAC	0	10	S4	K5
160	519.74	2	1038.473	1038.477	-3.73	{MTGSTETR]	alpha-NAC	0	8	0	dead-end	0	0	{0	x0
151	379.233	2	757.459	757.457	2.64	[NKAIR]	alpha-NAC	173	177	0	dead-end	0	0	K2	x0
147	527.739	2	1054.472	1054.472	-0.49	{mTGSTETR]	alpha-NAC	0	8	0	dead-end	0	0	{0	x0
134	471.275	2	941.543	941.541	1.56	[IGGKGTPR]	beta-NAC	23	30	0	dead-end	0	0	K4	x0
103	473.289	2	945.57	945.567	3.43	[IGGK]	beta-NAC	23	26	[GTPR]	beta-NAC	27	30	K4	T2
97	471.275	2	941.543	941.541	1.56	[IGGK]	beta-NAC	23	26	[GTPR]	beta-NAC	27	30	K4	T2
96	522.308	2	1043.609	1043.609	0.18	[KLANNVTK]	beta-NAC	123	130	0	dead-end	0	0	K1	x0
91	851.991	2	1702.974	1702.978	-2.29	[NILFVINKPDVFK]	alpha-NAC	87	99	0	dead-end	0	0	K8	x0
90	657.393	2	1313.778	1313.779	-0.76	[LGLKQVTGVSR]	alpha-NAC	69	79	0	dead-end	0	0	K4	x0

87	540.556	4	2159.201	2159.204	-1.38	[IGGKGTPR]	beta-NAC	23	30	[KLQAQQEHVR]	beta-NAC	13	22	K4	K1
87	851.993	2	1702.98	1702.978	1	[NILFVINKPDVFK]	alpha-NAC	87	99	0	dead-end	0	0	K8	x0
55	657.393	2	1313.778	1313.779	-0.76	[LGLK]	>sp|alpha	69	72	[QVTGVSR]	alpha-NAC	73	79	K4	T3
53	389.739	2	778.47	778.471	-0.92	[KLFSK]	alpha-NAC	64	68	0	dead-end	0	0	K1	x0
52	659.405	2	1317.803	1317.804	-0.69	[LGLK]	alpha-NAC	69	72	[QVTGVSR]	alpha-NAC	73	79	K4	T3
48	891.98	2	1782.952	1782.953	-0.89	[QAK]	alpha-NAC	52	54	[VAEAAGLGDHIDK]	alpha-NAC	39	51	K3	K13
47	541.561	4	2163.222	2163.229	-3.56	[IGGKGTPR]	beta-NAC	23	30	[KLQAQQEHVR]	beta-NAC	13	22	K4	K1
45	855.928	4	3420.689	3420.686	1.03	[DDGTVIHFNNPK]	beta-NAC	70	81	[VQTSVPANTFSVTGSADNK]	beta-NAC	82	100	K12	T3
42	586.376	2	1171.745	1171.745	-0.33	[KLFSKLGLK]	alpha-NAC	64	72	1	intrapeptidal	0	0	K1	K5
41	473.287	2	945.567	945.567	0.66	[IGGK]	beta-NAC	23	26	[GTPR]	beta-NAC	27	30	K4	T2
40	783.872	2	1566.736	1566.743	-4.55	[NETK]	beta-NAC	155	158	[NETKADEQ}	beta-NAC	155	163	K4	T3
36	433.452	5	2163.233	2163.229	1.42	[IGGKGTPR]	beta-NAC	23	30	[KLQAQQEHVR]	beta-NAC	13	22	K4	K1
29	480.293	2	959.579	959.577	2.02	[ALK]	alpha-NAC	178	180	[SEKK]	alpha-NAC	58	61	K3	K3
29	983.996	4	3932.961	3932.959	0.6	[SPGSDTYIIFGEAKIEDLTQHAQmSAIENLKPTR]	alpha-NAC	100	133	0	dead-end	0	0	T6	x0
28	796.984	2	1592.96	1592.964	-2.72	[VCIRK]	alpha-NAC	80	84	[VCIRKSK]	alpha-NAC	80	86	K5	K7
24	562.291	5	2807.424	2807.428	-1.29	{MmDSKAIAER]	beta-NAC	0	10	[TAAADDKKLQSNLK]	beta-NAC	39	52	{0	K8
24	839.19	4	3353.737	3353.741	-1.17	[KKVIHK]	beta-NAC	33	38	[LGPDGKGEDEDVPELVGDFDAASK]	beta-NAC	131	154	K2	K6
23	562.291	5	2807.424	2807.428	-1.29	{mMDSKAIAER]	beta-NAC	0	10	[TAAADDKKLQSNLK]	beta-NAC	39	52	{0	K8
22	983.994	4	3932.954	3932.959	-1.23	[SPGSDTYIIFGEAKIEDLTQHAQmSAIENLKPTR]	alpha-NAC	100	133	0	dead-end	0	0	Y7	x0

Intermolecular AtxQ78-NAC crosslinks.

Score	m/z	z	M+H+	Calculated	Deviation	Peptide 1	Protein 1	From	To	Peptide 2	Protein 2	From	To	Site 1	Site 2
45	632.035	3	1894.091	1894.084	3.54	[RKKK]	beta-NAC	31	34	[AIQLSmQGSSR]	Atx3 78Q	269	279	K3	S5
38	1026.208	3	3076.609	3076.594	4.83	[LGLK]	alpha-NAC	69	72	[NISQDMTQTSGTNLTSEELRKR]	Atx3 78Q	280	301	K4	S3
31	1158.192	3	3472.563	3472.554	2.37	[VQQmHRPK]	Atx3 78Q	200	207	[TVEEDENEDVEEDSTGIEEK]	alpha-NAC	140	159	K8	K20
25	772.085	3	2314.24	2314.245	-2.09	[SEKKAR]	alpha-NAC	58	63	[REAYFEKQQQK]	Atx3 78Q	302	312	K3	K7
25	767.06	3	2299.167	2299.165	0.86	[VQQMHRPK]	Atx3 78Q	200	207	{MTGSTETRQK]	alpha-NAC	0	10	K8	T7
21	790.709	3	2370.111	2370.11	0.57	[NETKADEQ}	beta-NAC	155	163	[EAYFEKQQQK]	Atx3 78Q	303	312	K4	K6
15	770.747	3	2310.227	2310.22	3.02	[SEKKAR]	alpha-NAC	58	63	[REAYFEKQQQK]	Atx3 78Q	302	312	K4	Y4
13	772.085	3	2314.241	2314.245	-1.65	[SEKKAR]	alpha-NAC	58	63	[REAYFEKQQQK]	Atx3 78Q	302	312	K4	K11
47	1066.949	5	5330.716	5330.718	-0.39	[LSVTNIPGIEEVNMIK]	beta-NAC	54	69	[NISQDMTQTSGTNLTSEELRKRREAYFEK]	Atx3 78Q	280	308	K16	K29
36	777.121	4	3105.46	3105.469	-2.73	{MMDSK]	beta-NAC	0	5	[NISQDMTQTSGTNLTSEELRK]	Atx3 78Q	280	300	{0	T7
35	777.121	4	3105.463	3105.469	-1.7	{MMDSK]	beta-NAC	0	5	[NISQDMTQTSGTNLTSEELRK]	Atx3 78Q	280	300	{0	S3
32	539.817	2	1078.628	1078.629	-1.58	[EVK]	alpha-NAC	11	13	[TEGKK}	Atx3 78Q	438	443	K3	K5
27	667.123	4	2665.471	2665.483	-4.83	[IGGKGTPR]	beta-NAC	23	30	[KRREAYFEKQQQK]	Atx3 78Q	300	312	T6	K1
24	1020.487	4	4078.928	4078.946	-4.37	[QAKQSR]	alpha-NAC	52	57	{SYYHHHHHHLENLYFQGMESIFHEK]	Atx3 78Q	0	25	K3	K25
20	667.123	4	2665.471	2665.483	-4.83	[IGGKGTPRRK]	beta-NAC	23	32	[REAYFEKQQQK]	Atx3 78Q	302	312	T6	K11
19	791.134	4	3161.513	3161.52	-2.25	[IGGKGTPR]	beta-NAC	23	30	[VLEANDGSGMLDEDEEDLQR]	Atx3 78Q	229	248	K4	S8
19	837.673	4	3347.669	3347.677	-2.16	[QAK]	alpha-NAC	52	54	[TFLQQPSGNmDDSGFFSIQVISNALK]	Atx3 78Q	77	102	K3	S17
18	837.675	4	3347.679	3347.677	0.75	[QAK]	alpha-NAC	52	54	[TFLQQPSGNmDDSGFFSIQVISNALK]	Atx3 78Q	77	102	K3	S22

Intramolecular AtxQ78 crosslinks.

Score	m/z	z	M+H+	Calculated	Deviation	Peptide 1	Protein 1	From	To	Peptide 2	Protein 2	From	To	Site 1	Site 2
106	561.65	3	1682.9	1682.932	-2.25	[LIGEELAQLKEQR]	Atx3 78Q	208	220	0	dead-end	0	0	K10	x0
61	385.21	3	1153.6	1153.621	2.17	[VHKTDLER]	Atx3 78Q	221	228	0	dead-end	0	0	K3	x0
54	799.71	3	2397.1	2397.109	0.61	[NISQDmTQTSGTNLTSEELR]	Atx3 78Q	280	299	0	dead-end	0	0	S10	x0
42	398.23	3	1192.7	1192.672	-1.01	[NDLK]	Atx3 78Q	434	437	[TEGKK}	Atx3 78Q	438	443	K4	T1
38	385.21	3	1153.6	1153.621	2.17	[VHK]	Atx3 78Q	221	223	[TDLER]	Atx3 78Q	224	228	K3	T1
37	396.89	3	1188.6	1188.647	-0.25	[NDLKTEGKK}	Atx3 78Q	434	443	0	dead-end	0	0	K4	x0
30	396.89	3	1188.6	1188.647	-0.25	[NDLK]	Atx3 78Q	434	437	[TEGKK}	Atx3 78Q	438	443	K4	T1
30	794.38	3	2381.1	2381.114	3.94	[NISQDMTQTSGTNLTSEELR]	Atx3 78Q	280	299	0	dead-end	0	0	T12	x0
27	500.62	3	1499.8	1499.848	-0.92	[TEGKK}	Atx3 78Q	438	443	[EQRVHK]	Atx3 78Q	218	223	K5	K6
25	767.06	3	2299.2	2299.165	0.86	[VQQMHRPK]	Atx3 78Q	200	207	{MTGSTETRQK]	alpha-NAC	0	10	K8	T7
22	398.23	3	1192.7	1192.672	0.1	[NDLK]	Atx3 78Q	434	437	[TEGKK}	Atx3 78Q	438	443	K4	K5
18	379.21	3	1135.6	1135.611	2.42	[VHKTDLER]	Atx3 78Q	221	228	1	intrapeptidal	0	0	K3	T4
17	386.55	3	1157.6	1157.646	-2.97	[VHK]	Atx3 78Q	221	223	[TDLER]	Atx3 78Q	224	228	K3	T1
115	577.31	2	1153.6	1153.621	-0.66	[VHKTDLER]	Atx3 78Q	221	228	0	dead-end	0	0	K3	x0
91	577.31	2	1153.6	1153.621	-0.66	[VHK]	Atx3 78Q	221	223	[TDLER]	Atx3 78Q	224	228	K3	T1
83	735.83	2	1470.6	1470.642	0.38	[MAEGGVTSEDYR]	Atx3 78Q	65	76	0	dead-end	0	0	S8	x0
77	735.83	2	1470.6	1470.642	1.24	[MAEGGVTSEDYR]	Atx3 78Q	65	76	0	dead-end	0	0	Y11	x0
75	841.97	2	1682.9	1682.932	0	[LIGEELAQLKEQR]	Atx3 78Q	208	220	0	dead-end	0	0	K10	x0
74	585.82	2	1170.6	1170.636	0.98	[NDLKTEGKK}	Atx3 78Q	434	443	1	intrapeptidal	0	0	K4	K8
73	667.12	4	2665.5	2665.482	-4.33	[VHKTDLER]	Atx3 78Q	221	228	[LIGEELAQLKEQR]	Atx3 78Q	208	220	T4	K10
71	743.82	2	1486.6	1486.637	-0.46	[mAEGGVTSEDYR]	Atx3 78Q	65	76	0	dead-end	0	0	S8	x0
70	573.32	4	2290.3	2290.259	-0.26	[VQQmHRPKLIGEELAQLK]	Atx3 78Q	200	217	0	dead-end	0	0	K8	x0
64	585.82	2	1170.6	1170.636	-1.5	[NDLKTEGKK}	Atx3 78Q	434	443	1	intrapeptidal	0	0	K8	T5
62	569.32	4	2274.3	2274.264	1.02	[VQQMHRPKLIGEELAQLK]	Atx3 78Q	200	217	0	dead-end	0	0	K8	x0
50	596.84	2	1192.7	1192.672	-2.71	[NDLK]	Atx3 78Q	434	437	[TEGKK}	Atx3 78Q	438	443	K4	T1
50	667.12	4	2665.5	2665.482	-4.33	[TDLER]	Atx3 78Q	224	228	LIGEELAQLKEQRVHK	Atx3 78Q	208	223	T1	K16
49	579.33	2	1157.6	1157.646	-0.73	[VHK]	Atx3 78Q	221	223	[TDLER]	Atx3 78Q	224	228	K3	T1
49	667.12	4	2665.5	2665.482	-4.33	[LIGEELAQLK]	Atx3 78Q	208	217	[EQRVHKTDLER]	Atx3 78Q	218	228	K10	T7
44	666.12	4	2661.4	2661.457	-3.24	[LIGEELAQLKEQRVHKTDLER	Atx3 78Q	208	228	0	dead-end	0	0	T17	x0
43	666.12	4	2661.4	2661.457	-3.24	[TDLER]	Atx3 78Q	224	228	LIGEELAQLKEQRVHK	Atx3 78Q	208	223	T1	K16
43	666.12	4	2661.4	2661.457	-3.24	[VHKTDLER]	Atx3 78Q	221	228	[LIGEELAQLKEQR]	Atx3 78Q	208	220	T4	K10
42	666.12	4	2661.4	2661.457	-3.24	[LIGEELAQLK]	Atx3 78Q	208	217	[EQRVHKTDLER]	Atx3 78Q	218	228	K10	T7
40	727.86	2	1454.7	1454.716	-0.8	[EAYFEKQQQK]	Atx3 78Q	303	312	0	dead-end	0	0	K6	x0
39	729.87	2	1458.7	1458.741	-3.95	[QQQK]	Atx3 78Q	309	312	[EAYFEK]	Atx3 78Q	303	308	K4	K6
36	743.82	2	1486.6	1486.637	1.5	[mAEGGVTSEDYR]	Atx3 78Q	65	76	0	dead-end	0	0	S8	x0
32	727.86	2	1454.7	1454.716	-0.8	[QQQK]	Atx3 78Q	309	312	[EAYFEK]	Atx3 78Q	303	308	K4	K6
27	675.34	2	1349.7	1349.673	0.79	[AIQLSmQGSSR]	Atx3 78Q	269	279	0	dead-end	0	0	S10	x0
27	667.34	2	1333.7	1333.678	-1.88	[AIQLSMQGSSR]	Atx3 78Q	269	279	0	dead-end	0	0	S10	x0
22	475.51	4	1899	1899.038	-1.93	[KRR]	Atx3 78Q	300	302	[EAYFEKQQQK]	Atx3 78Q	303	312	K1	K6

Table S2

Intra- and intermolecular NAC/Aβ40 crosslinks. Related to Figure 4 and Figure S4.

Score	m/z	z	M+H+	Calculated	Deviation	Peptide 1	Protein 1	From	To	Peptide2	Protein 2	From	To	Site 1	Site 2
231	756.419	2	1511.831	1511.832	-0.68	[LAEALPKQSVDGK]	beta-NAC	121	133	0	dead-end	0	0	K7	x0
175	730.889	2	1460.770	1460.767	2.48	[ETIMNQEKLAK]	beta-NAC	3	13	0	dead-end	0	0	K8	x0
169	512.315	3	1534.931	1534.918	8.75	[KVVHR]	beta-NAC	31	35	[IGGKGTAR]	beta-NAC	20	27	K1	K4
169	1149.282	4	4594.107	4594.148	-8.90	[LAEALPKQSVDGKAPLATGEDDDDEVPDLVENFDEASKNEAN}	beta-NAC	121	163	1	intrapeptidal	0	0	K7	K13
164	1156.810	4	4624.217	4624.234	-3.72	[LAEALPKQSVDGK]	beta-NAC	121	133	[APLATGEDDDDEVPDLVENFDEASKNEAN}	beta-NAC	134	163	K7	T5
161	495.954	3	1485.848	1485.850	-0.84	[AKQSR]	alpha-NAC	67	71	[IGGKGTAR]	beta-NAC	20	27	K2	K4
159	571.341	2	1141.675	1141.676	-0.75	[KAMSKLGLR]	alpha-NAC	78	86	1	intrapeptidal	0	0	K5	S4
156	539.954	3	1617.848	1617.844	2.63	[TATADDK]	beta-NAC	36	42	[IGGKGTAR]	beta-NAC	20	27	T1	K4
151	452.790	2	904.572	904.573	-0.50	[KKVVHR]	beta-NAC	30	35	1	intrapeptidal	0	0	K1	K2
151	1153.795	4	4612.157	4612.158	-0.32	[LAEALPKQSVDGKAPLATGEDDDDEVPDLVENFDEASKNEAN}	beta-NAC	121	163	0	dead-end	0	0	K13	x0
150	1156.808	4	4624.211	4624.234	-4.84	[LAEALPKQSVDGK]	beta-NAC	121	133	[APLATGEDDDDEVPDLVENFDEASKNEAN}	beta-NAC	134	163	K7	T5
148	458.268	2	915.528	915.526	2.40	[IGGKGTAR]	beta-NAC	20	27	0	dead-end	0	0	K4	x0
147	852.463	2	1703.919	1703.921	-1.23	[TATADDKKLQFSLK]	beta-NAC	36	49	1	intrapeptidal	0	0	K7	K8
145	1092.481	3	3275.428	3275.423	1.27	[APLATGEDDDDEVPDLVENFDEASKNEAN}	beta-NAC	134	163	0	dead-end	0	0	S24	x0
140	503.259	2	1005.511	1005.510	1.43	[TATADDKK]	beta-NAC	36	43	0	dead-end	0	0	K7	x0
136	559.643	3	1676.914	1676.918	-2.10	[IGGKGTAR]	beta-NAC	20	27	{MDAEFR]	Abeta40	0	6	K4	{0

135	677.733	3	2031.186	2031.189	-1.59	[KSKNILFVITKPDVYK]	alpha-NAC	98	113	1	intrapeptidal	0	0	K1	K3
134	499.607	3	1496.807	1496.807	-0.07	[KVVHR]	beta-NAC	31	35	[TATADDK]	beta-NAC	36	42	K1	T1
134	397.748	2	794.489	794.488	0.59	[KVVHR]	beta-NAC	31	35	0	dead-end	0	0	K1	x0
133	462.710	2	924.413	924.413	-0.35	{MDAEFR]	Abeta40	0	6	0	dead-end	0	0	{0	x0
132	502.942	3	1506.812	1506.812	-0.26	[AKQSR]	alpha-NAC	67	71	{MDAEFR]	Abeta40	0	6	K2	{0
131	512.311	3	1534.919	1534.918	0.62	[KVVHR]	beta-NAC	31	35	[IGGKGTAR]	beta-NAC	20	27	K1	K4
124	566.839	4	2264.333	2264.336	-1.42	[IGGKGTAR]	beta-NAC	20	27	[LAEALPKQSVDGK]	beta-NAC	121	133	K4	K7
123	510.309	2	1019.611	1019.614	-2.62	[KLQFSLK]	beta-NAC	43	49	0	dead-end	0	0	K1	x0
117	543.977	3	1629.917	1629.920	-1.54	[TATADDK]	beta-NAC	36	42	[IGGKGTAR]	beta-NAC	20	27	T1	K4
113	555.619	3	1664.842	1664.842	-0.08	[IGGKGTAR]	beta-NAC	20	27	{MDAEFR]	Abeta40	0	6	K4	{0
112	563.821	4	2252.263	2252.261	0.93	[IGGKGTAR]	beta-NAC	20	27	[LAEALPKQSVDGK]	beta-NAC	121	133	K4	K7
111	503.630	3	1508.877	1508.882	-3.58	[KVVHR]	beta-NAC	31	35	[TATADDK]	beta-NAC	36	42	K1	T1
111	470.707	2	940.406	940.408	-1.74	{mDAEFR]	Abeta40	0	6	0	dead-end	0	0	{0	x0
108	579.340	2	1157.672	1157.671	0.55	[KAmSKLGLR]	alpha-NAC	78	86	1	intrapeptidal	0	0	K5	S4
100	582.651	3	1745.937	1745.939	-1.29	[IGGKGTAR]	beta-NAC	20	27	[TATADDKK]	beta-NAC	36	43	K4	K7
98	384.484	4	1534.913	1534.918	-3.19	[KVVHR]	beta-NAC	31	35	[IGGKGTAR]	beta-NAC	20	27	K1	K4
96	406.979	4	1624.893	1624.902	-5.12	[KVVHR]	beta-NAC	31	35	[TATADDKK]	beta-NAC	36	43	K1	T1
96	499.980	3	1497.926	1497.925	0.87	[AKQSR]	alpha-NAC	67	71	[IGGKGTAR]	beta-NAC	20	27	K2	K4
93	586.676	3	1758.014	1758.015	-0.10	[IGGKGTAR]	beta-NAC	20	27	[TATADDKK]	beta-NAC	36	43	K4	K7
93	350.721	2	700.434	700.435	-1.97	[AKAVR]	alpha-NAC	193	197	0	dead-end	0	0	K2	x0

91	578.672	3	1734.001	1734.007	-3.49	[LQFSLK]	beta-NAC	44	49	[TATADDKK]	beta-NAC	36	43	S4	K7
91	574.651	3	1721.938	1721.932	3.64	[TATADDK]	beta-NAC	36	42	[LQFSLKK]	beta-NAC	44	50	T3	K6
88	449.262	2	897.517	897.515	2.32	[IGGKGTAR]	beta-NAC	20	27	1	intrapeptidal	0	0	K4	T6
73	360.702	2	720.397	720.396	0.95	[KAMSK]	alpha-NAC	78	82	0	dead-end	0	0	K1	x0
71	542.304	3	1624.898	1624.902	-2.13	[KVVHR]	beta-NAC	31	35	[TATADDKK]	beta-NAC	36	43	K1	K7
70	544.656	3	1631.954	1631.948	3.52	[LQFSLK]	beta-NAC	44	49	[IGGKGTAR]	beta-NAC	20	27	S4	K4
66	861.468	2	1721.929	1721.932	-1.67	[LQFSLK]	beta-NAC	44	49	[TATADDKK]	beta-NAC	36	43	S4	K7
57	554.072	4	2213.267	2213.271	-1.76	[IGGKGTAR]	beta-NAC	20	27	[ETIMNQEKLAK]	beta-NAC	3	13	K4	K8
51	820.919	2	1640.830	1640.835	-3.01	[LQFSLK]	beta-NAC	44	49	{MDAEFR]	Abeta40	0	6	S4	{0
42	446.264	2	891.521	891.519	3.15	[LQFSLK]	beta-NAC	44	49	0	dead-end	0	0	S4	x0
69	384.485	4	1534.917	1534.918	-0.32	[KVVHR]	beta-NAC	31	35	[IGGKGTAR]	beta-NAC	20	27	K1	K4
117	543.979	3	1629.923	1629.920	2.23	[TATADDK]	beta-NAC	36	42	[IGGKGTAR]	beta-NAC	20	27	T1	K4
68	563.821	4	2252.261	2252.261	-0.13	[IGGKGTAR]	beta-NAC	20	27	[LAEALPKQSVDGK]	beta-NAC	121	133	K4	K7
82	559.643	3	1676.913	1676.918	-2.64	[IGGKGTAR]	beta-NAC	20	27	{MDAEFR]	Abeta40	0	6	K4	{0
112	555.622	3	1664.851	1664.842	4.98	[IGGKGTAR]	beta-NAC	20	27	{MDAEFR]	Abeta40	0	6	K4	{0
80	1049.776	4	4196.082	4196.068	3.33	[LAEALPKQSVDGK]	beta-NAC	121	133	[APLATGEDDDDEVPDLVENFDEASK]	beta-NAC	134	158	K7	T5

Table S3

C. elegans strains. Related to STAR Methods.

DEU117	rmIs132 [*unc-54p*::Q35::YFP]; gamEx17 [*myo-3p*::empty::*unc-54* 3'UTR (50 ng/µl), *myo-2p*::mCherry::*unc-54* 3'UTR (2.5 ng/µl), DNA ladder (100 ng/µl)]
DEU118	rmIs132 [*unc-54p*::Q35::YFP]; gamEx18 [*myo-3p*::3xFLAG::αNAC::*unc-54* 3'UTR (25 ng/µl), *myo-3p*::3xFLAG::βNAC::*unc-54* 3'UTR (25 ng/µl), *myo-2p*::mCherry::*unc-54* 3'UTR (2.5 ng/µl), DNA ladder (100 ng/µl)]
DEU119	rmIs132 [*unc-54p*::Q35::YFP]; gamEx19 [*myo-3p*::3xFLAG::ΔUBA-αNAC::*unc-54* 3'UTR (25 ng/µl), *myo-3p*::3xFLAG::βNAC::*unc-54* 3'UTR (25 ng/µl), *myo-2p*::mCherry::*unc-54* 3'UTR (2.5 ng/µl), DNA ladder (100 ng/µl)]
DEU120	rmIs132 [*unc-54p*::Q35::YFP]; gamEx20 [*myo-3p*::3xFLAG::αNAC::*unc-54* 3'UTR (25 ng/µl), *myo-3p::*3xFLAG::RRK/AAA-βNAC::*unc-54* 3'UTR (25 ng/µl), *myo-2p*::mCherry::*unc-54* 3'UTR (2.5 ng/µl), DNA ladder (100 ng/µl)]
DEU121	rmIs132 [*unc-54p*::Q35::YFP]; gamEx21 [*myo-3p*::3xFLAG::αNAC::*unc-54* 3'UTR (25 ng/µl), *myo-3p*::3xFLAG::ΔNβ-NAC::*unc-54* 3'UTR (25 ng/µl), *myo-2p*::mCherry::*unc-54* 3'UTR (2.5 ng/µl), DNA ladder (100 ng/µl)]
DEU122	*marIs135 [unc-54p::*FlucDM::EGFP]; gamEx22 [*myo-3p*::empty::*unc-54* 3'UTR (50 ng/µl), *myo-2p*::mCherry::*unc-54* 3-UTR (2.5 ng/µl), DNA ladder (50 ng/µl)]
DEU123	*marIs135 [unc-54p::*FlucDM::EGFP]; gamEx23[*myo-3p*::3xFLAG::αNAC::*unc-43* 3'UTR (25 ng/µl), *myo-3p*::3xFLAG::βNAC::*unc-54* 3'UTR (25 ng/µl), *myo-2p*::mCherry::*unc-54* 3'UTR (2.5 ng/µl), DNA ladder (50 ng/µl)]
DEU124	*marIs135 [unc-54p::*FlucDM::EGFP]; gamEx24 [*myo-3p*::3xFLAG::αNAC::*unc-54* 3'UTR (25 ng/µl), *myo-3p*::3xFLAG::ΔNβ-NAC::*unc-54* 3'UTR (25 ng/µl), *myo-2p*::mCherry::*unc-54* 3'UTR (2.5 ng/µl), DNA ladder (50 ng/µl)]